



Bottom Current Modification of Turbidite Lobe Complexes

A. Fuhrmann^{1*}, I. A. Kane², E. Schomacker³, M. A. Clare⁴ and Anna Pontén⁵

¹Bavarian Environmental Agency, Hof, Germany, ²School of Earth, Atmospheric and Environmental Sciences, University of Manchester, Manchester, United Kingdom, ³Exploration and Production International, Equinor ASA, Fornebu, Norway, ⁴National Oceanography Centre, European Way, Southampton, United Kingdom, ⁵Research Centre Rotvoll, Equinor ASA, Trondheim, Norway

Submarine lobes form at the distal end of sediment gravity flow systems and are globally important sinks for sediment, anthropogenic pollutants and organic carbon, as well as forming hydrocarbon and CO₂ reservoirs. Deep-marine, near bed or bottom currents can modify gravity flow pathways and sediment distribution by directly interacting with the flow or by modifying seafloor morphology. Deciphering the nature of gravity- and bottom currents interaction, particularly in ancient systems, remains a challenge due to the lack of integrated datasets and the necessary oceanographic framework. Here we analyse high-resolution 3D seismic reflection and core data from the Upper Cretaceous interval offshore Tanzania to reveal the interaction of turbidite lobes with fine-grained sediment waves and contourite drift deposits. Contourite drift morphology governs the large-scale confinement style and shape of lobes that range from frontally confined and crescent shaped, to laterally confined and elongated, to semi-confined lobes. Core data reveals massive to cross-laminated high density turbidites in the lobe axis position that show no direct interaction between gravity flows and contour currents. Lobe off-axis and fringe deposits consist of parallel- and ripple-laminated, low density turbidites, which are inter-bedded with bioturbated, muddy siltstones that represent the toes of contourite drifts. Starved ripples, and streaks of up to fine-grained sandstone above individual turbidite beds indicate reworking by bottom currents. This facies distribution reflects the temporal interaction of quasi-steady bottom currents and turbidity currents that interact with the topography and build lobes over short periods of time. Frontally confined turbidity currents form lobes in a fill-and-spill fashion, in which the confinement of turbidity currents causes rapid deposition and obscures any bottom current signal. Lateral confinement causes increased turbidity current runout length, and promotes the development of lobe fringes with a high proportion of bottom current reworked sands. During times when sediment gravity flows are subordinate, contourites accumulate on top of the lobe, confining the next flow and thus modifying the overall stacking pattern of the lobe complex. Although sediment volumes of these bottom current modified lobe complexes are comparable to other deep-marine systems, bottom currents considerably influence facies distribution and deposit architecture.

Keywords: turbidite, contourite, lobe, deep-water, mixed system, ocean current, East Africa, Tanzania

OPEN ACCESS

Edited by:

Hajime Naruse,
Kyoto University, Japan

Reviewed by:

Maarten Van Daele,
Ghent University, Belgium
Naohisa Nishida,
Tokyo Gakugei University, Japan

*Correspondence:

A. Fuhrmann
ame.fuhrmann@zohomail.eu

Specialty section:

This article was submitted to
Sedimentology, Stratigraphy and
Diagenesis,
a section of the journal
Frontiers in Earth Science

Received: 02 August 2021

Accepted: 09 November 2021

Published: 21 February 2022

Citation:

Fuhrmann A, Kane IA, Schomacker E,
Clare MA and Pontén A (2022) Bottom
Current Modification of Turbidite
Lobe Complexes.
Front. Earth Sci. 9:752066.
doi: 10.3389/feart.2021.752066

1 INTRODUCTION

Submarine lobes form at the distal end of deep-marine sedimentary systems where they act as ultimate sink for vast amounts of sediment, organic matter and anthropogenic pollutants (Clift et al., 2001; Gwiazda et al., 2015; Kane and Clare, 2019). This makes them important archives for the reconstruction of past sediment budgets, climate and anthropogenic pollution, as well as reservoirs for hydrocarbons and carbon sequestration (Galy et al., 2007; Sømme et al., 2011; Bell et al., 2018a; Jobe et al., 2018; Rabouille et al., 2019; Pohl et al., 2020). Individual turbidite beds form lobes with predictable facies distributions; lobes then combine to build larger lobe complexes (Figure 1A) (Piper and Normark, 1983; Deptuck et al., 2008; Jegou et al., 2008; Prélat et al., 2009; Grundvåg et al., 2014; Marini et al., 2015; Kane et al., 2017; Sychala et al., 2017; Ferguson et al., 2020). Topography on continental slopes and basin floors can influence individual gravity flows, which in turn affects the ultimate geometry of their deposits (Figure 1B) (Kneller et al.,

1991; Kneller and McCaffrey, 1999; Sinclair and Tomasso, 2002; Al Ja'Aidi et al., 2004; Prélat et al., 2010; Bakke et al., 2013; Patacci et al., 2014; Salles et al., 2014; Doughty-Jones et al., 2017; Soutter et al., 2019; Howlett et al., 2019; Cumberpatch et al., 2021).

A growing body of research shows how deep-marine, margin parallel to oblique currents, here termed bottom currents, can play an important role in modifying turbidity current systems, but has mainly focused on proximal turbidite canyons and channels (McGinnis and Hayes, 1995; Faugères et al., 1999; Marchès et al., 2010; Brackenridge et al., 2013; Sansom, 2018; Fonnesu et al., 2020; Fuhrmann et al., 2020; Miramontes, et al., 2019). Little research has considered terminal lobes in these mixed systems, especially in terms of stratigraphic evolution, facies stacking patterns and the processes that control them (Locker and Laine, 1992; Marchès et al., 2010; Fonnesu et al., 2020). The processes that control turbidite-contourite interaction in distal, net-depositional systems likely differ from their proximal counterparts as they are subject to a lower frequency of high-concentration sediment-laden turbidity currents (Jobe

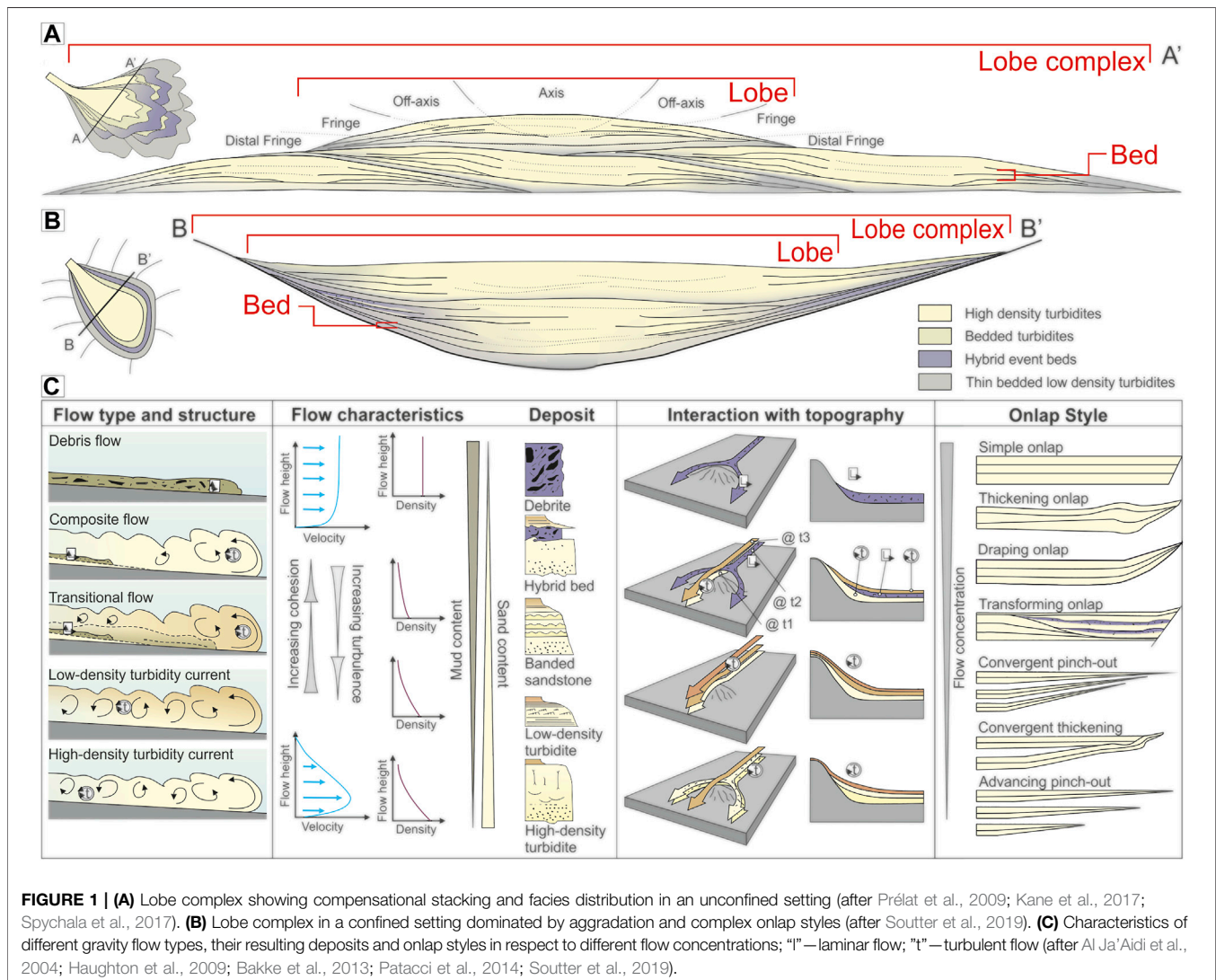
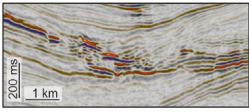
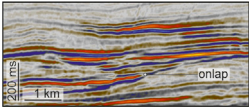
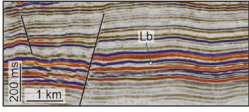
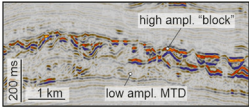
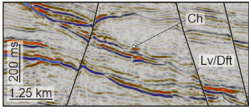
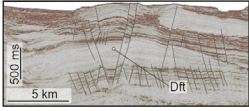
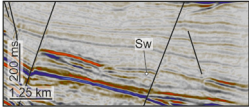
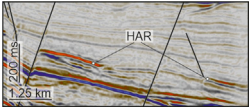


TABLE 1 | Seismic facies association defined for the sedimentary systems offshore Tanzania.

Seismic facies	Morphological association	Description/Interpretation	Seismic photograph
SFA 1	Slope channel complex fills	Discontinuous reflector with low- to high-, distorted amplitude reflectors at the base; stacked concave, discontinuous high amplitude reflectors with different degrees of confinement and sinuosity towards the top. Interpreted as sediment gravity flow sourced slope channel complexes; erosive base overlain by MTDs and stacked sandstone dominated channel complexes (Mayall et al., 2006).	
SFA 2	Lobe complexes (confined)	Parallel to sub-parallel high amplitude reflectors; on-lapping on topography, may show compensational stacking and draping onto relief. Interpreted as turbidity current sourced terminal lobe complexes deposited in a confined setting (Deptuk et al., 2008; Bakke et al., 2013; Soutter et al., 2019)	
SFA 3	Lobe complexes (unconfined)	Parallel to sub-parallel high amplitude reflectors; convex/positive relief; on-lapping on basal surface, may show compensational stacking. Interpreted as turbidity current sourced terminal lobe complexes forming without structural confinement (Deptuk et al., 2008; Prélat et al., 2009).	
SFA 4	Mass transport deposits (MTD)	Low- to high amplitude reflectors; slumped and contorted reflectors; zones of compression and extension may be observed. Interpreted as gravity induced failure of sediment, leading to sliding and slumping of sediments down-slope (Bull et al., 2009; Ortiz-Karpf et al., 2017).	
SFA 5	Hybrid levee-drifts (turbidite channel assoc.)	Asymmetrical, low amplitude, wedge shaped reflectors that are associated with turbidite channel fills (SFA 1); high amplitude channel fill interfingers with SFA 5. Interpreted as Hybrid levee-drift deposited by the interaction of margin parallel bottom currents and channelised turbidity currents (sensu Fuhrmann et al., 2020).	
SFA 6	Contourite drift deposits	Low amplitudes; large, convex sediment bodies; aggradational to migrational; faint to distorted, parallel to wavy reflectors with internal unconformities. Interpreted as contourite drifts of fine grained material deposited by "quasi-steady" margin parallel bottom currents. Internal facies changes reflect changes in bottom current flow regime (Faugeres et al., 1999)	
SFA 7	Low amplitude sediment waves	Wavy, parallel to sub-parallel, low amplitude reflectors, stepping up-slope with up to 45°; associated with the base of slope and basin floor. Interpreted as fine grained, up-current migrating sediment waves deposited as lee-waves by "quasi-steady" bottom currents (Flood, 1988; Wynn and Stow, 2002a)	
SFA 8	Channelised HAR	High amplitudes; non- to weakly erosive reflectors; filling topographic lows between low amplitude sediment waves. Interpreted as coarse-grained turbidites deposited in the topographic lows of low amplitude sediment waves (SFA 7) (sensu Bakke et al., 2013). Potentially reworked by margin parallel bottom currents.	

et al., 2018). Further potential for complex drift related topography along bottom current influenced margins (e.g., erosive moats and channels or depositional drifts and sediment waves) make distal lobe complexes prone to increasingly passive turbidite-contourite interaction (Hernández-Molina et al., 2008; Mulder et al., 2008). An excellent location to study such systems is the East African Margin as long-lived bottom current systems from Mesozoic to modern time build extensive contourite drift deposits that locally interact with point sourced turbidite systems (Sansom, 2018; Thiéblemont et al., 2019; Thiéblemont et al., 2020). Excellent data quality allows us to image deposits in detail and record variations over time, and to conclusively link deposits to their seismic character.

We use high-resolution 3D seismic reflection data in combination with biostratigraphically constrained well-log and core data from offshore Tanzania to reveal the diversity of bottom current influence on gravity flow pathways and lobe geometries, which arise from spatio-temporal fluxes in available sediment supply, near-bed current

intensity and the frequency of lobe-building flows. Our specific aims are to: 1) document the stratigraphic evolution of bottom current influenced lobe complexes that were deposited offshore Tanzania during the Upper Cretaceous; 2) establish the different factors controlling lobe morphology and facies stacking patterns; and 3) develop a generalised model to explain how gravity flows of varying types interact with different contourite drift morphologies along continental margins.

2 DATA AND METHODS

This study uses two 3D seismic reflection volumes covering the Sea Gap (4,885 km²) and Davie Ridge (3,240 km²), offshore Tanzania, at a present day water depth of approximately 2,200–2,500 m. The 3D seismic reflection volumes were correlated with a 2 D seismic tie-line (Figure 2C, Figure 4). The data have a bin spacing of 12.5 × 12.5 m, a 4 ms sampling rate and are processed in SEG normal polarity to zero

TABLE 2 | Facies Associations encountered in Well B and D offshore Tanzania.

Lithofacies	Description	Interpretation	Environment
LF 1 Massive sandstone (dewatered)	Poorly sorted, medium grained, thick amalgamated sandstone with increased amount of mud at bed bases and granule sized mud clasts. Individual beds transition from massive to well-developed banding and abundant dewatering structures (dishes and pillars) towards the bed tops	Structureless amalgamated sandstone beds are interpreted to be deposited by high density turbidites in lobe axis position (Lowe, 1982; Prélat et al., 2009; Grundvåg et al., 2014; Marini et al., 2015; Kane et al., 2017). The strong dewatering and large variety of grain sizes suggest a deposition by rapid flow deceleration (Lowe, 1975; Porten et al., 2019)	Lobe axis (Fa1)
LF 2 Cross-laminated Sandstone	Medium grained, thick amalgamated massive to parallel- and cross- stratified sandstone. Cross stratification commonly steepens and cross cuts each other. Granule sized mud-clasts and rare dewatering structures may occur	Structureless amalgamated sandstone beds are interpreted to be deposited by high density turbidites in lobe axis position (Lowe, 1982; Prélat et al., 2009; Grundvåg et al., 2014; Marini et al., 2015; Kane et al., 2017). Traction structures indicate a deposition by continuous flow rather than abrupt freezing (Kneller & Branney, 1995)	Lobe axis (Fa1)
LF 3 Bedded sandstone	Well bedded, fining-up, medium to fine grained sandstone beds that transition from massive to parallel-and ripple- laminated with often well-developed bed tops that transition into LF 4 and 5. Laminae and ripple foresets are often muddy and distorted leading to convolute lamination	Interpreted to be deposited as waning low density turbidites along lobe- off-axis and -fringe position. (Prélat et al., 2009; Grundvåg et al., 2014; Marini et al., 2015; Kane et al., 2017; Spychala et al., 2017). Convolute lamination and muddy foresets indicate flow interaction with basin internal relief and/or margin parallel bottom currents (Martin-Chivelet et al., 2008; Tinterri et al., 2016)	Lobe off-axis to lobe fringe (Fa2)
LF 4 Banded sandstone	Medium to fine grained, well sorted sandstone interbedded with dark, muddy, organic rich, poorly sorted sandstone that cause a colour banding	Temporal transition from laminar to turbulent flows due to entrainment of cohesive mud at the base of the flow (Baas et al., 2009; Sumner et al., 2009; Kane & Pontén, 2012). May be caused by deceleration of turbidity current along depositional relief (Barker et al., 2008; Patacci et al., 2014) or flow run-outs (Kane et al., 2017)	Base of Lobe axis (Fa1) or hybrid beds along Lobe off-axis (Fa2)
LF 5 Clay rich, non stratified sandstone and slumped thin- beds	Mudstones and diamicts interbedded with convolute deformed sandstone beds and injectites. Clasts with preserved individual turbidite beds may occur	These are interpreted as local slumps or debrites along basin topography along the lobe- off-axis and -fringe (Armitage et al., 2009; Ortiz-Karpf et al., 2017; Spychala et al., 2017; Soutter et al., 2019)	Debrites/slumps along lobe off-axis to lobe fringe (Fa3)
LF 6 Reworked, graded silt- to fine grained sandstone	Interbedded, fine grained, parallel- to ripple-laminated sandstones and laminated or bioturbated muddy siltstones. Thin sand streaks and starved ripples at bed tops and graded bed bases are common	Turbidite bed that were reworked by bottom currents. Coarsening and fining trends along bed base and tops may represent the variability of bottom currents (Martin-Chivelet et al., 2008; Fuhrmann et al., 2020)	Bottom current reworked lobe fringe (Fa3)
LF 7 (Faint) laminated to mottled muddy siltstone	Thick deposits of mudstone or muddy siltstone that is strongly bioturbated. Faint lamination and coarsening and fining grain-size trends may be preserved locally	Thick mudstone successions deposited by waxing and waning of "quasi-steady" bottom currents (<i>sensu</i> Stow and Faugères, 2008; Brackenridge et al., 2018)	Contourite drift deposit (Fa4)

phase, where a peak (yellow colour) represents a downward increase in acoustic impedance. The average vertical resolution is 20–30 m in the Upper Cretaceous, with an average dominant frequency of 40 Hz and internal velocities of 2.5–3.5 km s⁻¹. A total of 14 biostratigraphically controlled exploration wells and 1.2 km of core are available to calibrate the seismic data and interpret the sedimentary evolution (Table 1, Table 2). Seismic interpretation was conducted by creating semi-automatic horizon stacks with Paleoscan™ that were manually adjusted with the available well data in Petrel™. The resulting seismic stratigraphic framework from Albian to Neogene consists of eight characteristic, basin wide seismic horizons that represent major unconformities, stratal terminations or extensive changes in seismic facies (Data rep. Table 1). This framework allows a correlation with previously-documented

tectonic events, palaeo-oceanographic events and regional bottom current circulation patterns (Figure 2) (Castelino et al., 2016; Fischer and Uenzelmann-Neben, 2018a; Sansom, 2018; Thiéblemont et al., 2020). Seismic attribute volumes, such as Root Mean Square (RMS) amplitude extractions, variance blends (VAR), spectral decomposition Red-Green-Blue (RGB) colour blends, thickness maps and seismic cross sections are used to interpret the sedimentary systems of each interval. Geoteric™ is used to transform the seismic data into the frequency domain using the Constant Q method to maintain high vertical resolution, which allowed for the identification of subtle lithology changes in interbedded deposits (McArdle and Ackers, 2012). The resulting seismic facies associations are then used to define eight deep-marine sedimentological features (Table 1).

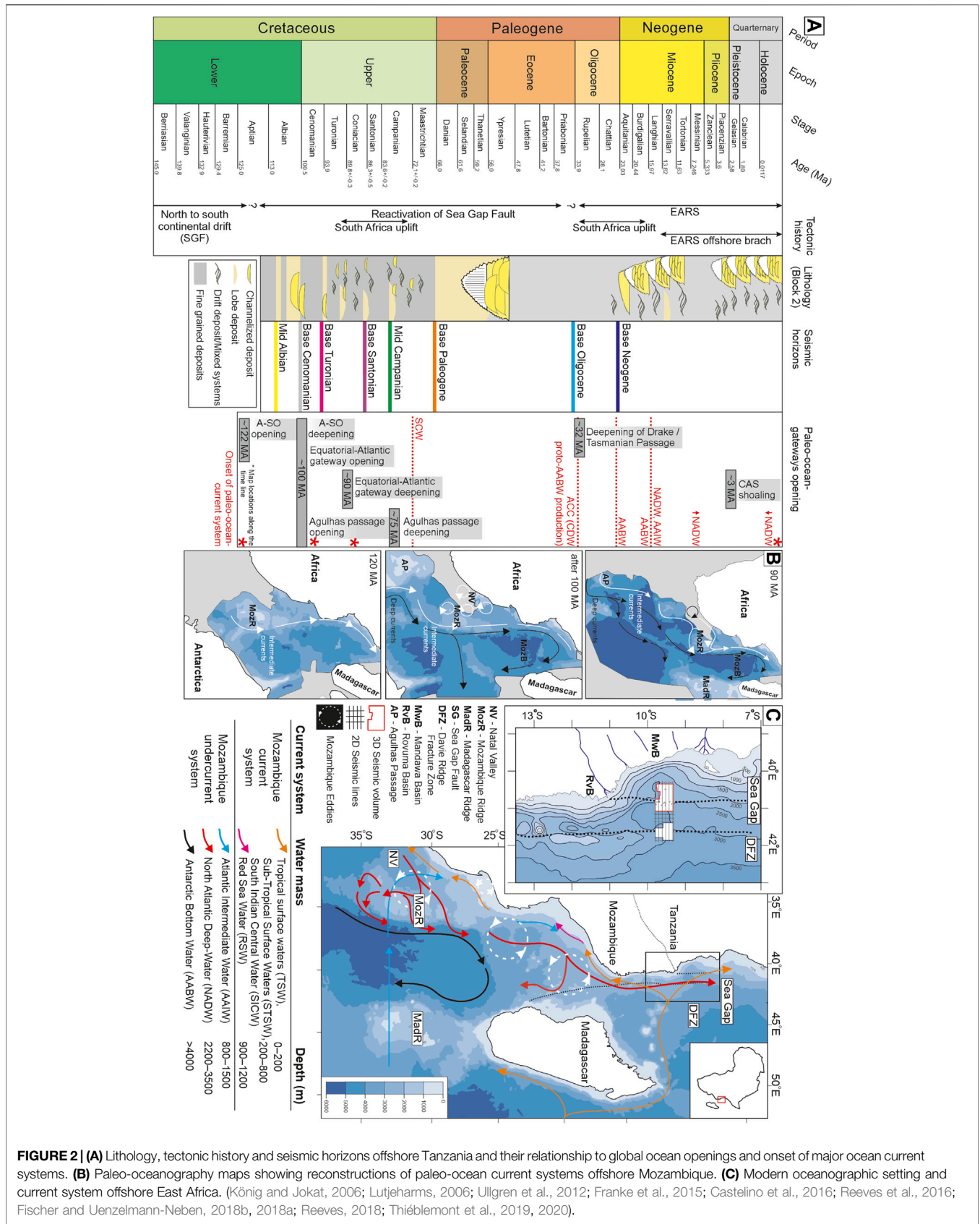


FIGURE 2 | (A) Lithology, tectonic history and seismic horizons offshore Tanzania and their relationship to global ocean openings and onset of major ocean current systems. **(B)** Paleogeography maps showing reconstructions of paleo-ocean current systems offshore Mozambique. **(C)** Modern oceanographic setting and current system offshore East Africa. (König and Jokat, 2006; Lutjeharms, 2006; Ullgren et al., 2012; Franke et al., 2015; Castelino et al., 2016; Reeves et al., 2016; Fischer and Uenzelmann-Neben, 2018b, 2018a; Reeves, 2018; Thiéblemont et al., 2019, 2020).

The Cenomanian, Santonian and mid-Campanian intervals show the distinct influence of margin-parallel bottom currents on deep marine lobe complexes and were directly targeted by two drill cores (total length of 70 m). Detailed logging of the cored deposits enabled the identification of individual lithofacies types (LF 1–7) that are grouped into four facies associations according to their associated depositional processes (FA) (**Table 2**; **Figure 3**). Individual deposits were linked to regional-scale oceanographic processes to investigate the temporal variability of down- and along-slope processes. Lobe size, morphology and facies distribution are further compared to a global compendium of lobes from confined and unconfined systems (Prélat et al., 2010) to investigate similarities and differences to gravity-current dominated deep-marine sedimentary systems.

3 GEOLOGICAL AND OCEANOGRAPHIC SETTING

3.1 Basin Evolution and Sedimentology

Northwest-southeast oriented rifting that overprinted initial failed rifts (Karoo rifts) during the Late Jurassic to Lower Cretaceous led to the breakup of the Gondwana Supercontinent and the development of the East African Coastal Basins (**Figure 2**) (Salman and Abdula, 1995; Leinweber and Jokat, 2012; Reeves et al., 2016; Reeves, 2018). The separation of eastern- (Madagascar, India, Antarctica and Australia) and western- Gondwana (Africa and America) caused the development of shallow marine sedimentary systems in the Mandawa and Rovuma Basins (Key et al., 2008; Smelror et al., 2008, 2018; Hudson and Nicholas, 2014; Fossum et al., 2019). The initial rifting was followed by north to south continental drift along two large transform fault zones, the Davie Ridge and the Sea Gap, during the Kimmeridgian and Barremian (Reeves et al., 2016). Continental drift ceased with the onset of rifting between Madagascar and India, but subsequent reactivation of these lineaments formed considerable tectonic relief in the form of pull-apart mini-basins and pop-up structures during the Upper Cretaceous (Salman and Abdula, 1995; Reeves et al., 2016). A transgression in the Albian caused the development of deep-marine sedimentary systems in East African Offshore Basins (Key et al., 2008; Smelror et al., 2008, 2018; Sansom, 2018; Fossum et al., 2019). Tectonic movement along the Sea Gap (SG) and drift deposition by margin parallel, northwards flowing deep-marine currents caused the development of extensive topography along the margin (Sansom, 2018; Thiéblemont et al., 2020). This topography and direct interactions of margin-parallel currents greatly influence local turbidite systems, causing asymmetrical morphologies and facies distribution along submarine channel-fills and lobe complexes (Sansom, 2018; Fonnesu et al., 2020; Fuhrmann et al., 2020). Sediment was sourced by long-lived sediment entry points along old rift shoulders of failed Karoo-rifts, and large river systems such as the Rovuma and Rufiji (Key et al., 2008; Smelror et al., 2008; Fossum et al., 2019). Pulses of coarse grained sediment in the Late Albian, Middle-Late Cenomanian, Early Turonian and Early Santonian caused channel incision and the deposition of coarse-grained deposits at the base of slope which are the focus of this study.

3.2 Cretaceous Oceanographic Setting

Ocean current circulation developed prior to the Albian, but was sluggish and locally restricted (Robinson et al., 2010; Voigt et al., 2013). The progressive subsidence of the Drake Passage, the formation of a deep-water connection between the South Atlantic Ocean and the Indian Ocean, and the opening of the Atlantic in the Cenomanian (about 100 Ma) caused a reorganisation of the global circulation system and ventilation of the Southern Ocean (Poulsen et al., 2001; König and Jokat, 2006, 2010). The driving mechanism of ocean circulation is debated, but meridional overturning of circulation during peak Cretaceous greenhouse temperatures is suggested (Murphy and Thomas, 2012). Continuous opening of the Agulhas passage allowed inflow of surface (Upper Pacific Water, Upper North Atlantic Water) and intermediate waters (Intermediate Southern Ocean Water) into the Indian Ocean (Uenzelmann-Neben et al., 2017) (**Figure 2B**). This gateway opening time correlates with the onset of bottom current-related sedimentation in the Mozambique and Tanzanian coastal basins (Sansom, 2018; Thiéblemont et al., 2020). Palaeo-bathymetric reconstructions of the Mozambique Channel and the Riiser Larsen Sea indicate strong, erosive, northward-flowing bottom currents at paleo-depths of about 900–1,500 m or shallower in the Cenomanian to Campanian (Castelino et al., 2016; Fischer and Uenzelmann-Neben, 2018a) (**Figure 2B**). The interval of most intense bottom currents likely correlates with the onset of global cooling after the Cretaceous Thermal Maximum in Turonian times (~91 Ma), which caused a gradual increase of the temperature gradient between poles and equator (Poulsen et al., 2001, 2003; Friedrich et al., 2012; Murphy and Thomas, 2012). This time is marked by non-deposition in northern Mozambique and extensive contourite drift development offshore Tanzania, indicating a northwards extension of these currents (Sansom, 2018; Thiéblemont et al., 2020). A weakening of bottom currents from the Campanian (~75 Ma) onwards caused contourite deposition along the Mozambique Ridge and the Mozambique Channel and a cessation of bottom current related sedimentation along the upper slope, east of the Sea Gap offshore Tanzania (Fischer and Uenzelmann-Neben, 2018a; Sansom, 2018; Fuhrmann et al., 2020; Thiéblemont et al., 2020) (**Figure 2B**). This weakening of currents was caused by major reorganisation of the ocean current system due to further subsidence of the Agulhas Plateau and Rio Grande Rise/Walvis Ridge System (Robinson et al., 2010; Martin et al., 2012; Murphy and Thomas, 2012, 2013; Robinson and Vance, 2012; Donnadieu et al., 2016; Moiroud et al., 2016).

4 RESULTS

Here we describe the sedimentological evolution of lobe complexes in the Cenomanian, Santonian and Campanian.

4.1 Seismic Facies Associations

Large-scale observations and interpretations are based on the eight seismic facies associations (SFA 1 to 8 in **Table 1**) that were defined based on distinct differences in internal seismic character and bounding seismic horizons. Core calibrated gamma ray logs from four wells (Well A to D) are used to infer grain size characteristics of the drift deposits, submarine channel- and lobe complexes.

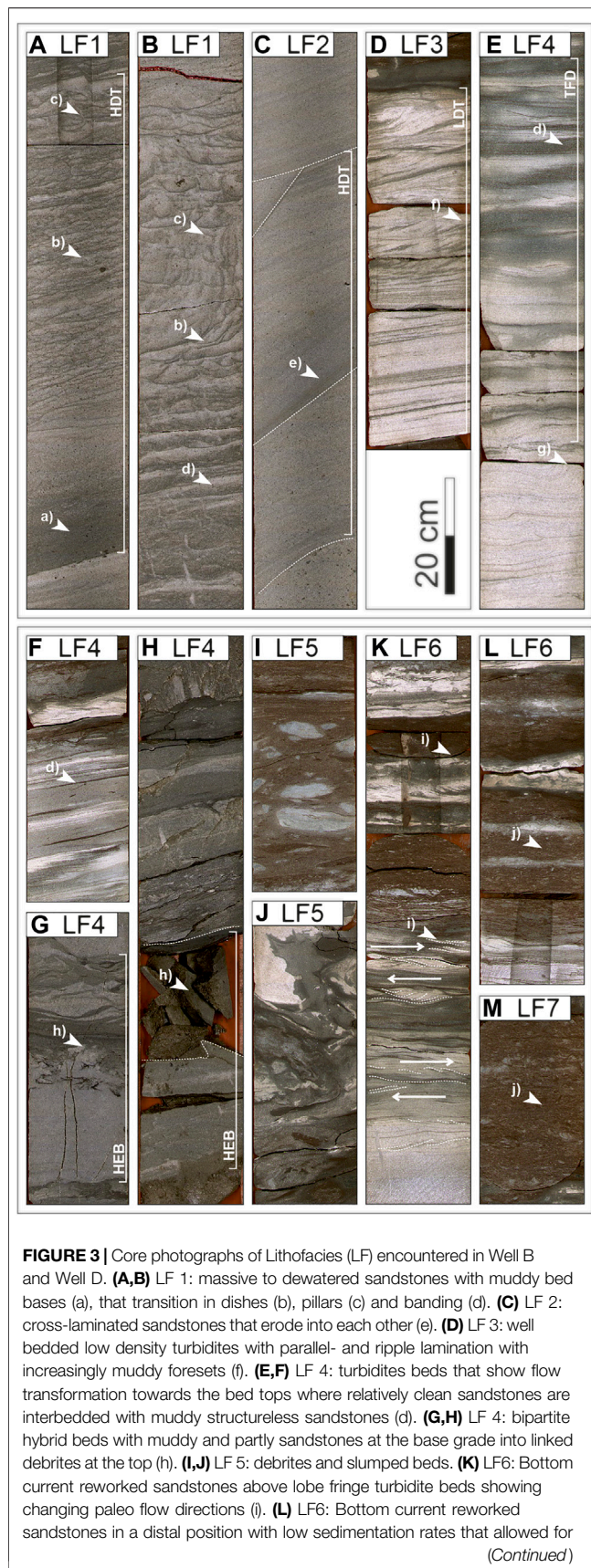


FIGURE 3 | Core photographs of Lithofacies (LF) encountered in Well B and Well D. **(A,B)** LF 1: massive to dewatered sandstones with muddy bed bases (a), that transition in dishes (b), pillars (c) and banding (d). **(C)** LF 2: cross-laminated sandstones that erode into each other (e). **(D)** LF 3: well bedded low density turbidites with parallel- and ripple lamination with increasingly muddy foresets (f). **(E,F)** LF 4: turbidites beds that show flow transformation towards the bed tops where relatively clean sandstones are interbedded with muddy structureless sandstones (d). **(G,H)** LF 4: bipartite hybrid beds with muddy and partly sandstones at the base grade into linked debrites at the top (h). **(I,J)** LF 5: debris and slumped beds. **(K)** LF 6: Bottom current reworked sandstones above lobe fringe turbidite beds showing changing paleo flow directions (i). **(L)** LF 6: Bottom current reworked sandstones in a distal position with low sedimentation rates that allowed for (Continued)

FIGURE 3 | pervasive bioturbation (j). **(M)** LF 7: Drift deposit consists of mottled, red to green muddy siltstones. HDT—High density turbidites; LDT—Low density turbidites; TFD—Transitional flow deposits; HEB—Hybrid event beds.

4.2 Facies Associations

Bed scale observations are based on 70 m of core recovered from Well B and Well D that target the lobe complexes in the Cenomanian and mid-Campanian (**Figures 3, 5, 7**). Seven lithofacies types (LF 1–7) are grouped into four facies associations (Fa 1–4) according to their associated depositional processes to understand the bottom current influence of lobe sub-environments (**Table 2**).

4.2.1 Fa 1: Lobe Axis

4.2.1.1 Observation

Facies association 1 consists of thick amalgamated, dewatered- and cross laminated sandstone (LF 1 and 2) and subordinate banded sandstone (LF 4) (**Figures 3A,B,C**). LF 1 is composed of poorly sorted, medium-grained sandstones. Subtle grain size changes at the base indicate erosive, up to 2 m thick beds that transition from massive, muddy sandstones into a banded fabric (LF 4) with mud prone dishes and pillars at the top (**Figure 3A**). Pillars and undersides of dishes are mud free and often carbonate cemented. The banded sandstones (LF 4) are made up of 1–2 cm thick interbedded intervals of clean sandstones and dark, muddy, organic-rich poorly sorted sandstone. Cross laminated sandstones (LF2) are medium grained, moderately sorted and dominated by low to high angle cross lamination that steepens up and cross cuts each other. Individual beds may be mud rich at the base and clean towards the top. Granule sized mud clasts are common throughout the succession.

4.2.1.2 Interpretation

The erosional bases, high degree of amalgamation and poor sorting indicate that the sandstones were deposited rapidly by high density turbidity currents that experienced a sudden loss of flow capacity (Lowe, 1982; Hiscott, 1994). The observed banding suggests erosive flows that underwent flow transformation when the entrained mud increased the cohesiveness of the flow (Lowe and Guy, 2000; Sumner et al., 2009; Baas et al., 2011; Kane and Pontén, 2012; Stevenson et al., 2020). Rapid deposition in combination with the entrained mud causes the formation of local overpressured pore waters that breach through mud rich laminae and develop dish and pillar structures (Lowe, 1975). Locally “flushed” pore space along the undersides of dishes and within pipes facilitate the precipitation of carbonate cement (Southern et al., 2017; Porten et al., 2019). The more massive to cross laminated sandstone indicates deposition by high density turbidity currents along traction carpets that change from grain fallout and tractional deposition (Kneller and Branney, 1995). Increasing angles along cross beds may result from long wavelength dunes (low angle cross beds) or scours that were backfilled with high angle cross beds and supercritical flow conditions in narrow, lateral confined basins (Arnott and Al-Mufti, 2017). These sedimentary characteristics are commonly associated with axial positions in depositional lobes and confined

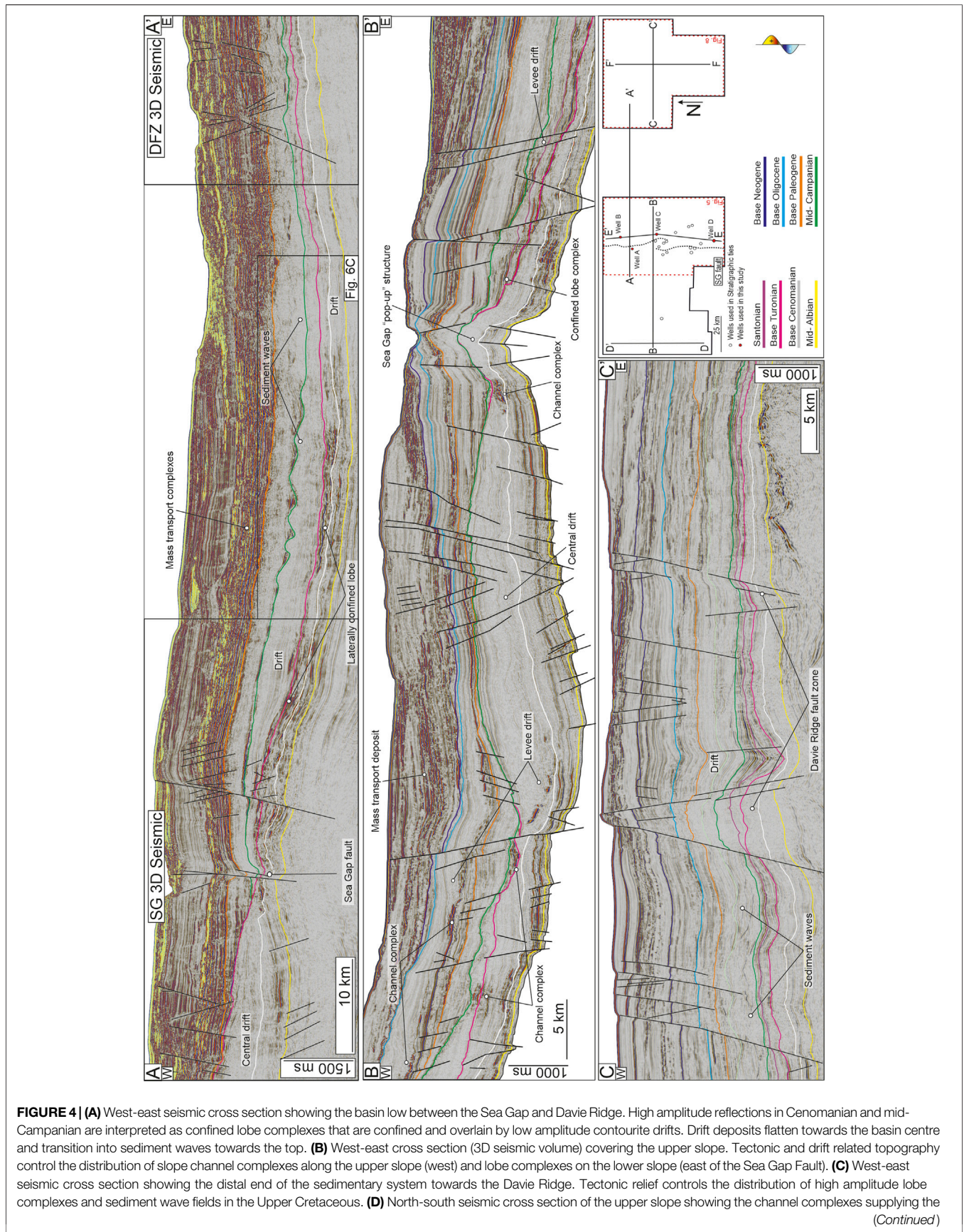


FIGURE 4 | deep-marine sedimentary system with coarse-grained sediment in the Upper Cretaceous (yellow to orange seismic horizon). Note the strong interaction of low amplitude contourite drift deposits with the high amplitude channel fill. **(E)** North-south seismic cross section along the lower slope/break of slope showing high amplitude lobe complexes between low amplitude contourite drift deposits. The target of this study are the high amplitude lobes complexes in the Cenomanian (white seismic horizon), Turonian to Santonian (purple seismic horizons) and Mid-Campanian (green seismic horizon) that are targeted by Well B, C and D. **(F)** North-south cross section of the Davie Ridge area showing the distal expression of high amplitude lobes and HAR interacting with contourites.

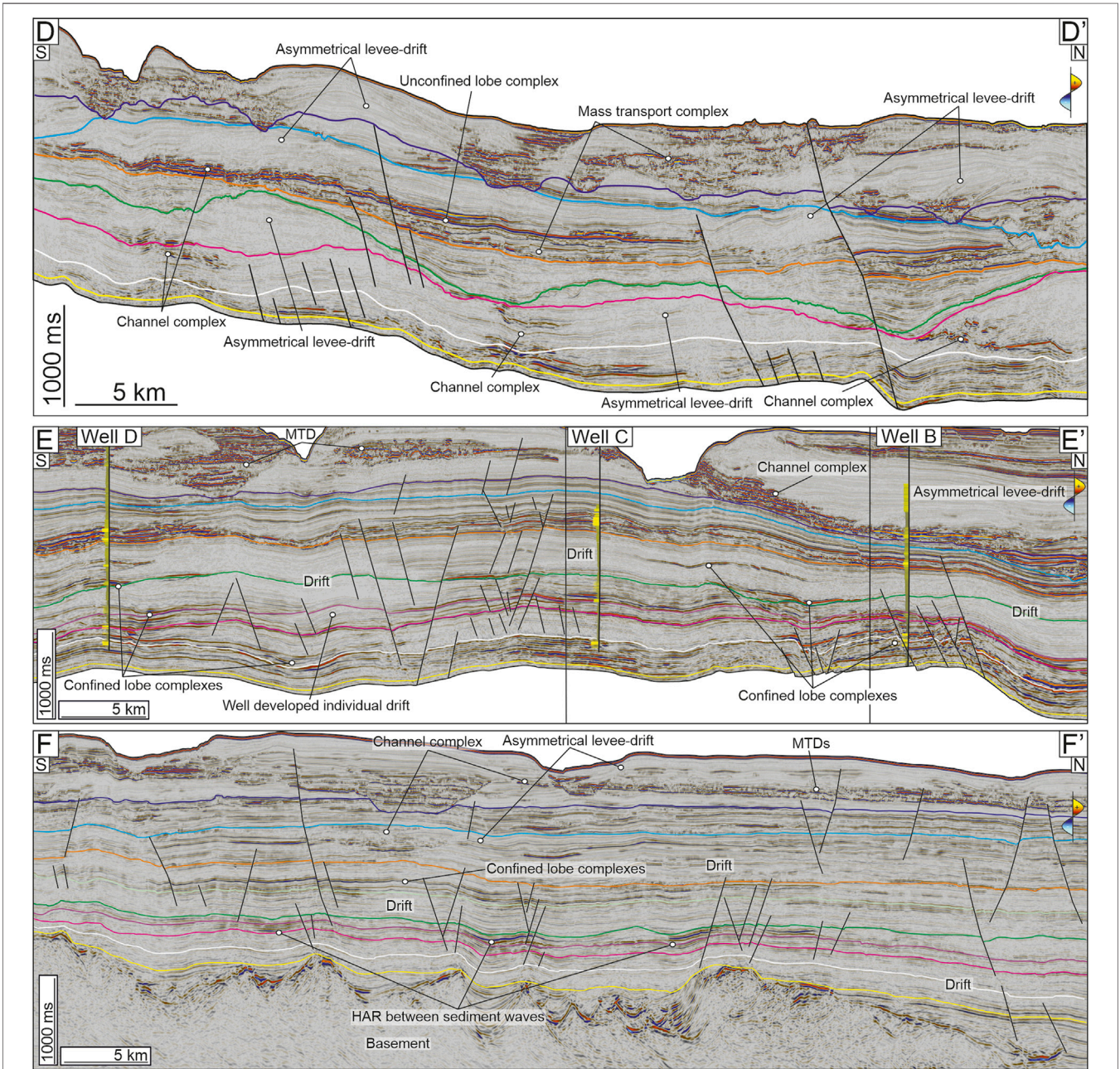


FIGURE 4 | (Continued).

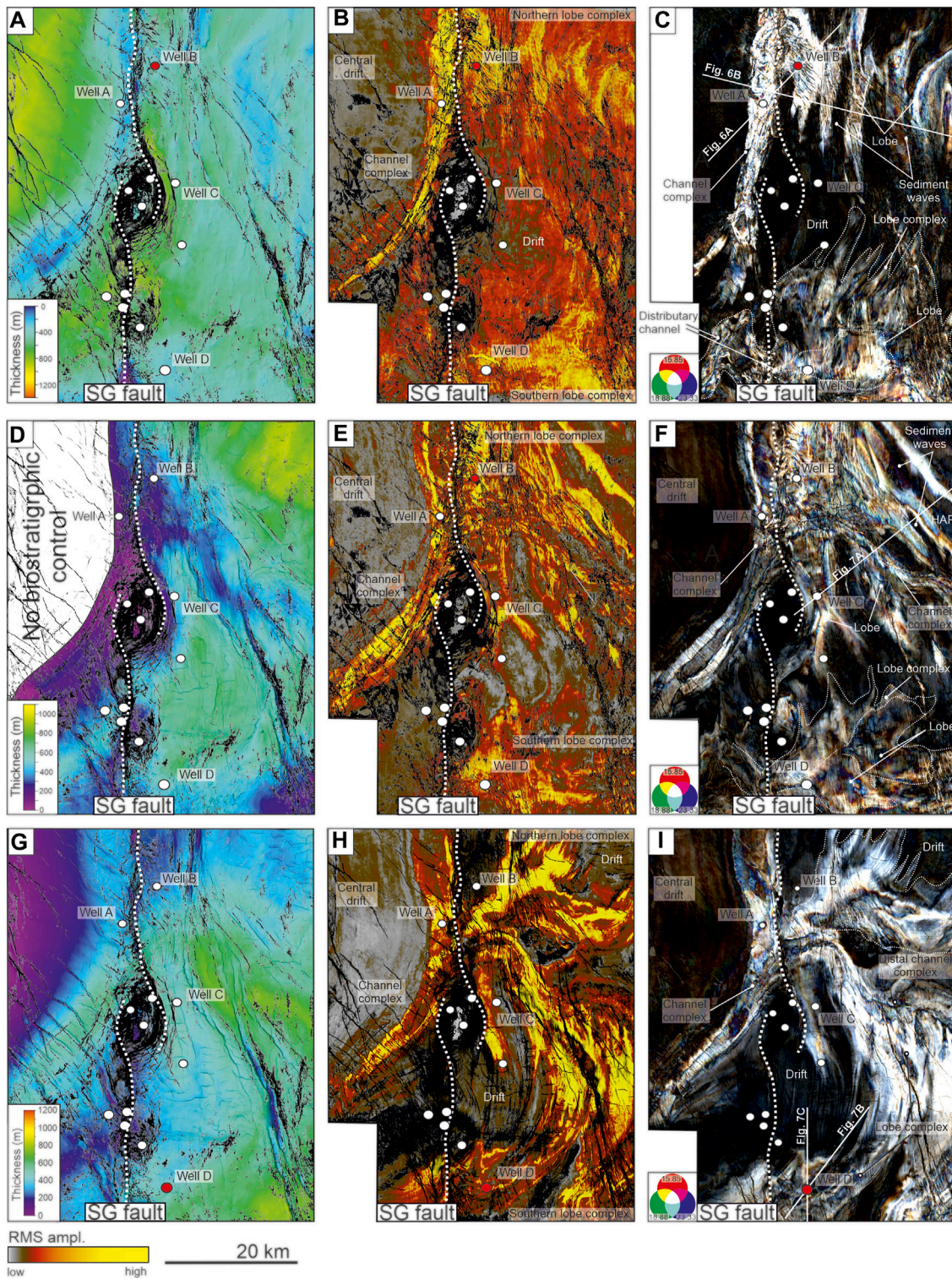


FIGURE 5 | (A–C) Cenomanian Lobe complexes east of the SG fault. **(A)** Thickness map of the Cenomanian to Turonian (white to purple seismic horizon). **(B)** Root mean square amplitude (RMS) extraction of the same interval shows the distribution of coarse-grained sediments. **(C)** Spectral decomposition image showing the dimming and confinement of high amplitude (bright) reflectors interpreted as lobe complexes onto the low amplitude drift deposits. Cross sections A and B are shown in **(D–F)** Santonian lobe complexes east of the SG fault. **(D)** Thickness map shows the thickness interval of the Turonian to mid-Campanian. **(E)** RMS amplitude extraction showing the distribution of coarse grained sediments. **(F)** Spectral decomposition shows the distribution of high amplitude lobes, sediment waves and distal slope channel complexes. Note how the relief of low amplitude drift deposits, control the overall distribution of high amplitude turbidite deposits and well developed *(Continued)*

FIGURE 5 | amplitude dimming towards the lobe fringes. **(G–I)** mid-Campanian lobe complexes east of the SG fault. **(G)** Thickness map shows the thickness interval of the Turonian to mid-Campanian. **(H)** RMS amplitude extraction showing the distribution of coarse grained sediments. **(I)** Spectral decomposition shows the detailed distribution of high amplitude lobes that drape and interact with the low amplitude contourite drift deposits in the northeast and southwest. Note the well-developed distributary channels and dimming of high amplitudes draping onto the low angle drift deposits.

settings (Grundvåg et al., 2014; Hansen et al., 2019; Soutter et al., 2019).

4.2.2 Fa 2: Lobe Off-Axis to Proximal Fringe

4.2.2.1 Observation

Medium bedded (0.1–1.2 m thick), normally-graded, medium to fine grained sandstones (LF 3), with subordinate banded sandstones (LF 4), slumped beds and debrites (LF 5) (**Figures 3D,E,I,J**). Bed bases are sharp to slightly erosive, loaded and often associated with cm scale injectites. Individual beds transition from massive to parallel-, ripple- and convolute-laminated towards the top. Increased mud content is observed within individual beds and is often focussed along ripple-forests and parallel-laminae. Where mud content in the matrix increases, beds show banding as well as rare dish and pillar structures (LF 4). Banded sandstones consist of ripple lamination that are interbedded with structureless mud-rich sandstones that gradually transition into each other. Beds in the lower part of the cored section in Well B (**Figure 6A**, Zoom I) show up to 20 cm thick muddy, medium grained sandstones that are banded or show strong dewatering that are directly overlain by structureless, clast rich debrites (**Figures 3G,H**). Core damage limits the quality of observation, but small rip up clasts indicate the overlying debrites are linked to the sandstone below.

4.2.2.2 Interpretation

The sharp to erosive bed bases, massive to tractional sedimentary structures and normal grading indicates that the beds of LF 3 were deposited by waning turbidity currents (e.g. Bouma, 1962). Initial deposition of massive sandstones was followed by constant tractional reworking as flows became more dilute (Lowe, 1982; Mulder and Alexander, 2001). Convolute lamination and injectites are linked to flows encountering topography, which is evident at seismic scale (**Figure 6**, **Figure 7** and **Figure 8**), causing flow deflection, disruption of sedimentary structures and bed internal opposing paleo current indicators (**Figures 3E,K** arrows) (Kneller et al., 1991; McCaffrey and Kneller, 2001; Tinterri et al., 2016; Cobain et al., 2017). The banded sandstones result from flows that transition from turbulent to laminar “regimes” due to the increased entrainment of cohesive clay into the flow and the formation of laminar plugs within the flow (Baas et al., 2009; Sumner et al., 2009). An increase in mud was likely caused by erosion of muddy substrate along gentle relief or rapid deposition of the coarse grained sediment fraction in the flow (Kane and Pontén, 2012; Kane et al., 2017; Southern et al., 2017). Linked debrites in Well B are interpreted as hybrid beds that form due to high mud entrainment rates or flow deceleration along basin internal relief (Haughton et al., 2003, 2009; Talling, 2013; Patacci et al., 2014; Fonnesu et al., 2015). Traction structures within turbidite beds, and local flow transformation indicate deposition in an off-axis to proximal lobe fringe position away from the focal point of sediment gravity flows in a weakly to strongly confined

environment (Prélat et al., 2009; Spychala et al., 2017; Soutter et al., 2019) (**Figure 1**).

4.2.3 Fa 3: Bottom Current Reworked Lobe Fringe

4.2.3.1 Observation

Thin bedded (1–10 cm), sharp based, normally graded, fine grained sandstones are dominated by ripple- and local convolute-lamination (LF 3) and are overlain by rhythmically stacked fine-grained sandstones and muddy reddish-brown to grey siltstones (LF 6 and 7) (**Figure 3K–M**). These overlying fine-grained sand- and siltstones consist of individual streaks and starved ripples that show a sharp or gradual basal contacts with inverse to normal grading. Mud rich ripple-foresets and laminae indicate different paleocurrent directions compared to the underlying beds (**Figure 3K**). Bioturbation is common and may be pervasive in thin beds that are embedded in fine-grained muds of LF 5 (**Figure 3L**).

4.2.3.2 Interpretation

The sharp based and normally graded thin beds are interpreted to be deposited by dilute turbidity currents under constant tractional reworking (Best and Bridge, 1992; Mulder and Alexander, 2001; Jobe et al., 2012). These beds are commonly encountered in lateral lobe fringes where relatively dilute flows wane away from the axis of the deposits (Prélat et al., 2009; Spychala et al., 2017; Hansen et al., 2019). The thin, fine-grained sand- and siltstone succession above individual beds are interpreted to represent a complex interplay of local flow deflection, mud entrainment and tractional reworking of fine-grained turbidite sands by bottom currents. These currents may form trains of starved ripples within muddy fine sand- and siltstones at flow velocities of around $0.3 \text{ m}^{\ast\ast-1}$ (Masson et al., 2004; Stow et al., 2009). Different paleo-current directions in respect to underlying beds may to some extent be caused by flow deflection of turbidity currents along local topography, but is also considered an indication of the influence of margin parallel bottom currents (Shanmugam et al., 1993; Martín-Chivelet et al., 2008). Seismic scale observations and bottom current activity during the time of deposition (Thiéblemont et al., 2020) support the reworking of sands by bottom currents (*sensu de Castro et al., 2020*). Grain-size variations and gradual to sharp bed bases are likely related to variability bottom current velocity (de Castro et al., 2020). Decreasing sedimentation rates towards the most distal lobe fringe, correlate with pervasive bioturbation that often obscures the primary sedimentary structures and no sorting is recognisable, similar to commonly observed contourite facies (Stow and Faugères, 2008; Brackenridge et al., 2018).

4.2.4 Fa 4: Contourite Drifts

4.2.4.1 Observation

This facies association consists of reddish-brown to greenish-grey muddy siltstone that is between 10 cm and 1.5 m thick (LF 7). Deposits are mottled with locally preserved faint lamination of up

to fine-grained sandstone (Figure 3M). Bed bases are diffuse, transitioning upwards from bottom current reworked sandstones (Fa 3) (Figures 3K, L). Subtle grain-size changes indicate a gradual coarsening then fining throughout the otherwise homogenous beds.

4.2.4.2 Interpretation

The poorly sorted siltstones are interpreted to be deposited by waxing and waning bottom currents during the absence of sediment gravity flows (Gonthier et al., 1984; Stow and Faugères, 2008; Brackenridge et al., 2018). Deposition rates are inferred to be relatively low, which allows for pervasive bioturbation to take place (Figure 3M). The relatively silty character of the deposits suggests bottom current flows of about $0.3 \text{ m}\cdot\text{s}^{-1}$, which increased temporally during the transport of fine grained sand (Hollister and McCave, 1984; McCave et al., 2017; Thrane et al., 2018). Seismic scale observation (Figures 4, 6, 7, 8) indicate that these “toes” of the contourite drifts migrate onto and interfinger with turbidite lobe off-axis and fringe deposits.

4.3 Cenomanian

4.3.1 Seismic Scale Observations of Frontally Confined Lobes

Extensive contourite drifts (SFA 6) that form along tectonic relief associated with the Sea Gap and Davie Ridge (Figure 4) dominate the deep-marine sedimentary system in the Cenomanian. Slope channel complex fills (SFA 1) that are confined by drift deposits (SFA 5) and tectonic relief (Figures 4B,E) extend into high amplitude lobe complexes (SFA 2) north and south of the Sea Gap pop-up structure (Figure 4E, Figure 5A–C). In the north, the lower slope is dominated by low amplitude sediment waves (SFA 7) (maximum thickness of ~100 m and 3 km width) that follow the curved contours of the slope. Lobe complexes fill the topographic lows of sediment waves represented by overlapping high amplitude reflectors onto the low amplitude reflectors of the sediment waves (Figures 6A,B). Lobes are narrow and elongated with average widths of 3 km, length of 19 km and thicknesses up to 100 m (Figure 6B zoom). Sharp amplitude contrasts of RGB colour blends along the fringes indicate steep confinement and poorly-developed thin bedded lobe fringe facies (Figure 5C). Narrow, up to 500 m wide, high amplitude/frequency responses connect each crescent-shaped lobe complex and are interpreted as sediment entry points indicating frontal erosion and sediment transport from one topographic low to another (Figure 5C). Southwest stacking of sediment waves cause a lateral offset of confined lobes over time and governs the lobe complex stacking pattern (Figure 6B, zoom II). The southern depo-centre is dominated by ~ 5 km wide drift deposits (SFA6) that step up the slope and are pinned to the tectonic relief of the Sea Gap (Figures 5A,B,C, Figure 7A). High amplitude reflectors show well-developed lobate shapes (length > width) that onlap and drape onto the relatively gentle dipping flanks of contourite drift deposits. High amplitude distributary channels feed into individual high amplitude lobes that dim gradually away from the lobe axes indicating well-developed lobe-off-axis and lobe fringe facies (Figure 5C). 2D seismic lines display the extension of small drifts and sediment wave fields into the basin low between the

Sea Gap and Davie Ridge, indicating similar confinement styles along the distal part of the sedimentary system (Figure 4A, Figure 6C). Spectral decomposition images of the eastern 3D seismic survey displays elongated northwest striking, high amplitude reflectors between straight crested, low amplitude sediment waves in the west of the Davie Ridge, that represent the most distal part of the turbidite system (Figures 8A,C). The dimming of amplitudes suggests a decrease in grain-size towards the distal end of the sedimentary system.

4.3.2 Bed-Scale Observations Frontally Confined Lobes

High amplitude seismic reflectors in the Cenomanian interval are targeted by four wells (Well A, B, C and D in Figure 5, Figure 6A, Figure 7). Low, blocky gamma ray log responses of Well A to D of coarse-grained sediments correspond to the high-amplitude reflectors forming the deep-marine sedimentary system (Figures 3, 9). Frontally confined lobe complexes in the north, penetrated by Well B, show blocky low GR signatures, indicating about 100 m thick sandstones deposited in the topographic lows between the sediment waves (Figures 6A,B). A total of 33 m of core (blue box in Figure 6A, zoom I) shows a basal interval of hybrid beds that represent lobe off-axis deposits (Fa 2) along the topographic confinement (Figure 9A). This interval is overlain by thick amalgamated, poorly-sorted, medium-grained high density turbidites that are deposited in an axial position (Fa 1) (Figure 5C). Individual beds are tentatively identified by increased mud content at the base that transitions into banding and abundant dish and pillar structures towards the top (LF 1). Sandstone beds clean towards the top of the succession and develop low to high angle cross bedding that steepens over an interval of 10–30 cm (LF 2). Mud caps are generally absent from the upper part of the succession.

4.4 Santonian

4.4.1 Seismic Scale Observations on Laterally Confined Lobes

The contourite depositional system along the base of slope (east of the Sea Gap) changed during the Santonian. The northern depocentre is dominated by northwest-southeast striking, straight crested, sediment waves (SFA 7) with wavelengths of up to 5 km (width ~2.5 km and a height of ~100 m) (Figures 5E,F, Figure 7A). Associated with their topographic lows are high amplitude reflectors that onlap and drape over the topography (SFA 8). Through the Santonian and early Campanian, these sediment waves transition into large drift deposits of parallel, continuous, low amplitude reflectors that extend towards the Davie Ridge with maximum thicknesses of ~1,650 m in Well B (total drift thickness from Santonian to base Paleogene) (Figure 4A, Figure 5D). A northwest-southeast striking, distal channel complex (SFA 1) interacts with this drift (SFA5) (Figure 5F, Figure 7A). High amplitude reflectors extend from the channel and dim towards the northwest where they interfinger with low amplitude reflectors of the large drift (Figure 7A). Smaller drift deposits of 10–15 km width are developed further south where they are pinned to the eastern

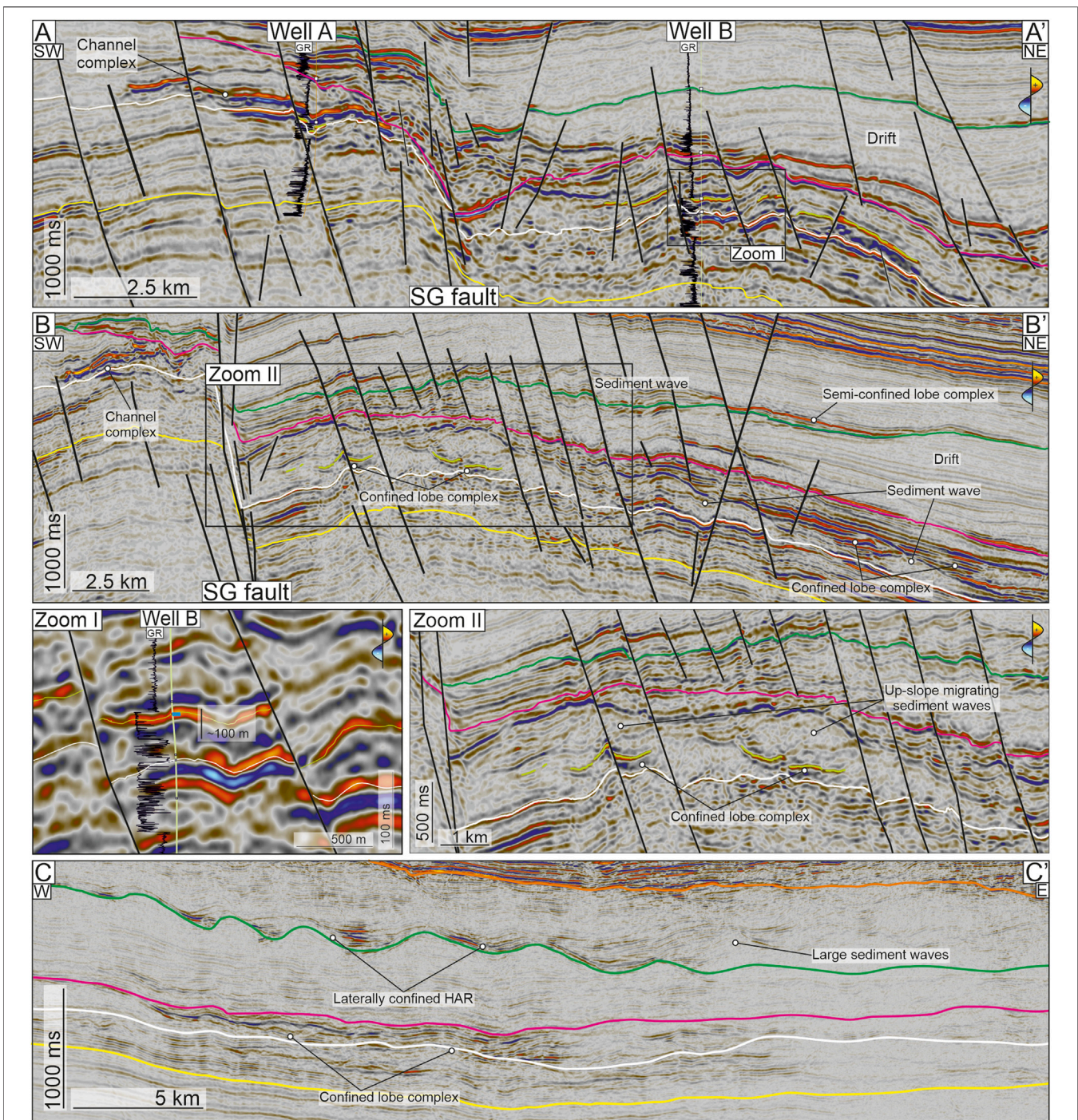


FIGURE 6 | Seismic cross-sections east of the SG showing confined lobe complexes of the Cenomanian. **(A)** Feeder channel confined by the large central drift and SG (targeted by Well A) and the correlated drift confined lobe complex. The green seismic horizon represents the cored interval. Zoom I shows the blocky GR signature and cored interval (blue bar) of Well B. **(B)** High amplitude lobe complexes confined by sediment waves. Zoom II shows the lateral confinement and southwest migrating sediment waves stepping over the confined lobe complexes. **(C)** 2D line in the west of the 3D seismic volume shows the extension of confined high amplitude reflectors into the basin. Location is shown in **Figures 5A–C**.

side of the Sea Gap pop-up structure, and form a moat along the topographic high (**Figure 7A**, zoom I). Along the southern depocentre these drift deposits are onlapped and draped by high amplitude reflections of a lobe complex (SFA 2) with a

length of ~30 km and a width of ~19 km (**Figure 4E**, **Figure 5F**). Well-developed internal seismic morphologies show up to 500 m wide distributary channels that connect individual lobes (**Figure 5F**). Amplitude dimming indicates well-developed

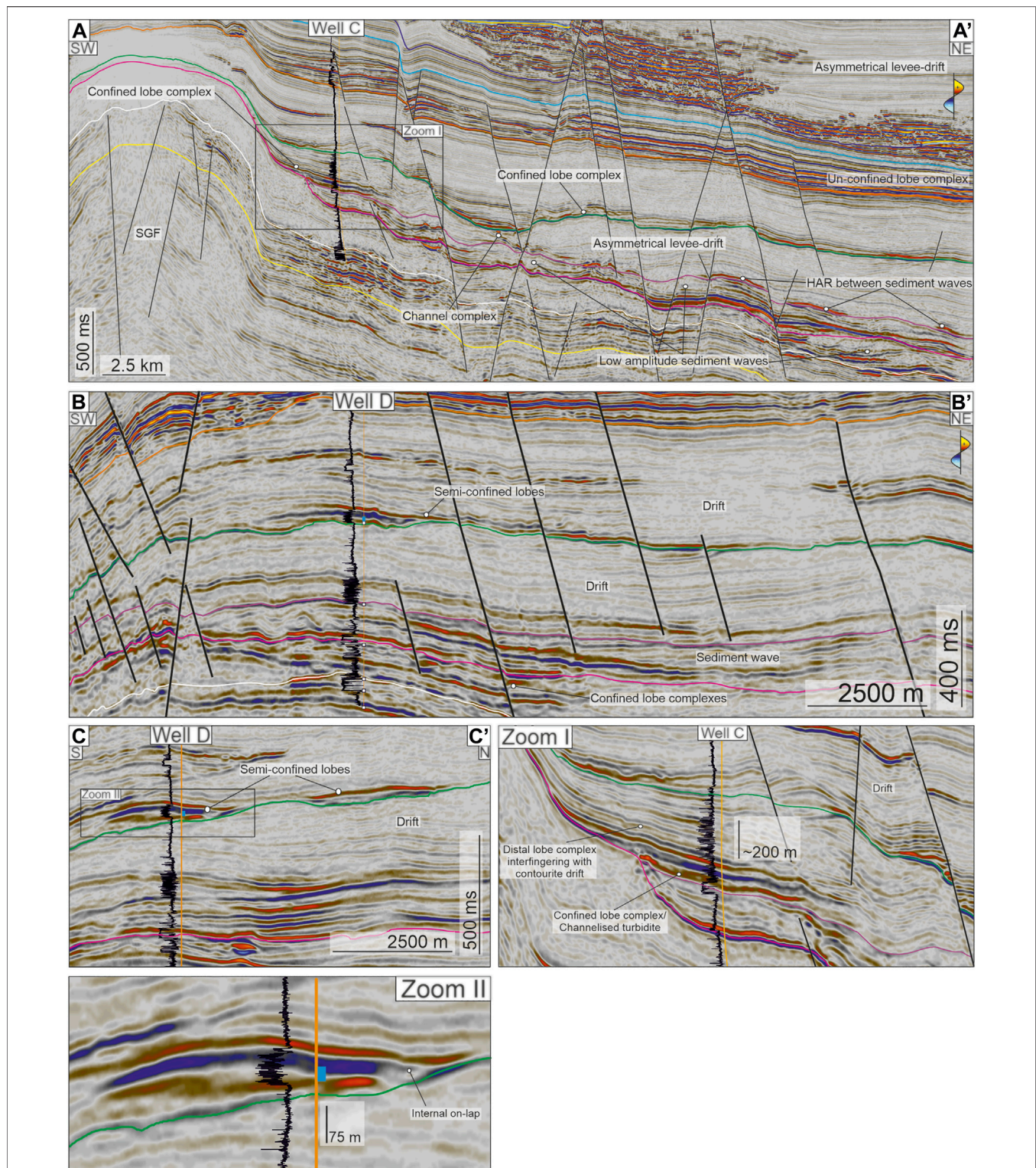


FIGURE 7 | (A) Seismic cross section showing the distribution of HAR between low amplitude sediment waves in the Santonian (dark purple pick) and a distal slope channel complex with a well-developed asymmetrical levee-drift to the north. Well C targeting confined lobe complexes developed between up-slope migrating drift deposits and the Sea Gap Fault. Zoom I: Spiky GR signatures suggested interbedded mud and coarse-grained sediments. **(B)** Southwest to northeast cross section shows the one-sided lateral on-lap surface of the lobe complex on low amplitude drift deposits. **(C)** Well D targeting the laterally confined lobe complexes. Zoom II shows the spiky GR signature and cored interval (blue bar) of Well D. Location of cross sections in **Figures 5C–I**.

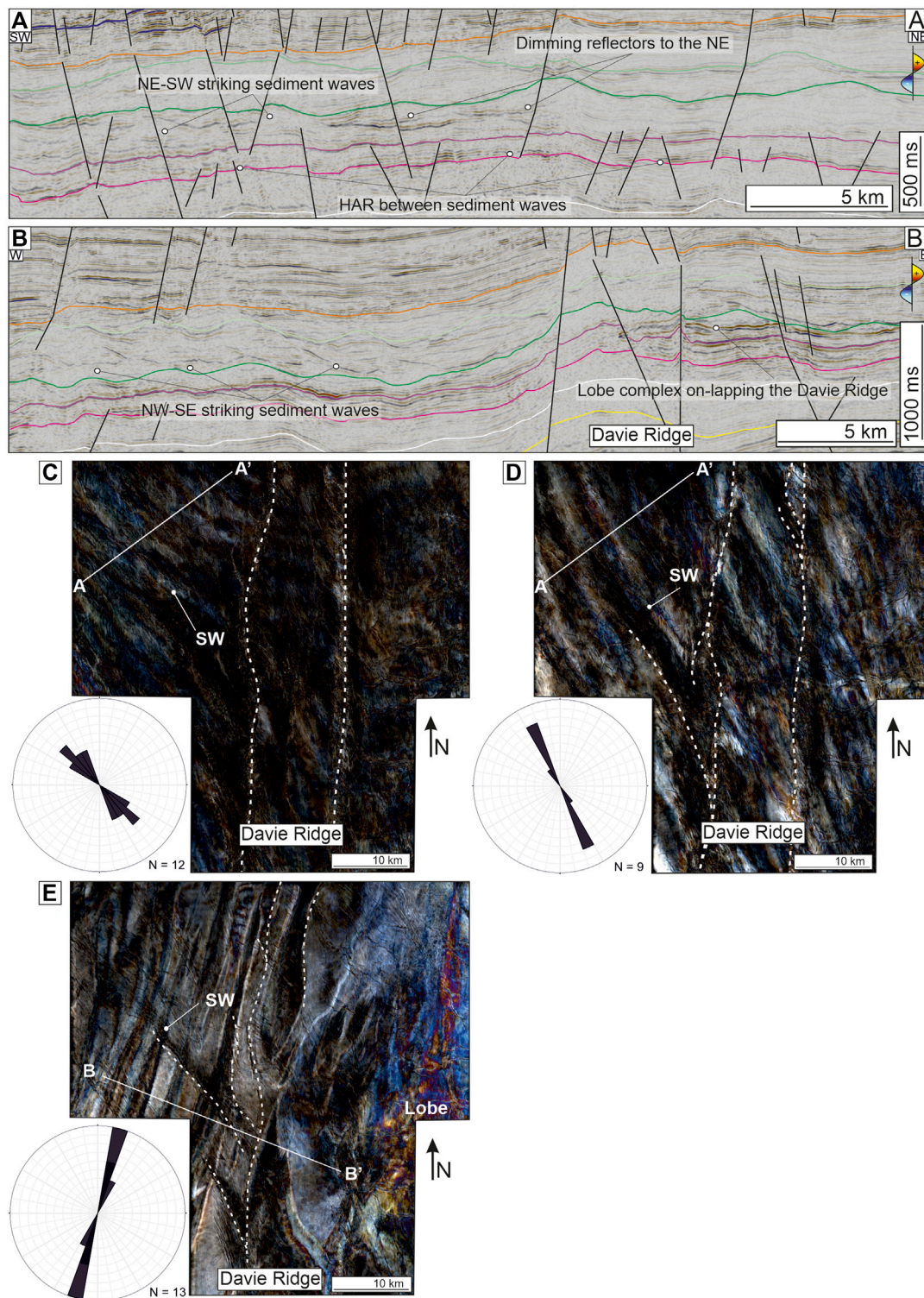


FIGURE 8 | (A) Southwest to northeast cross section covering high amplitudes that are associated with the topographic lows of sediment waves along the Davie Ridge. **(B)** Northwest to southeast cross section showing the well-developed sediment wave field in the mid-Campanian in the east of the Davie Ridge. High amplitude associated with the topographic lows of these sediment waves are interpreted as the most distal expression of the turbidite system offshore Tanzania. **(C–E)** Spectral decomposition maps of the Cenomanian **(C)**, the Santonian **(D)** and mid-Campanian **(E)**. HARs are interpreted as coarse-grained sediment associated with the topographic lows of sediment waves. Note the change of sediment wave orientation during the Santonian **(D)** and mid-Campanian **(E)**.

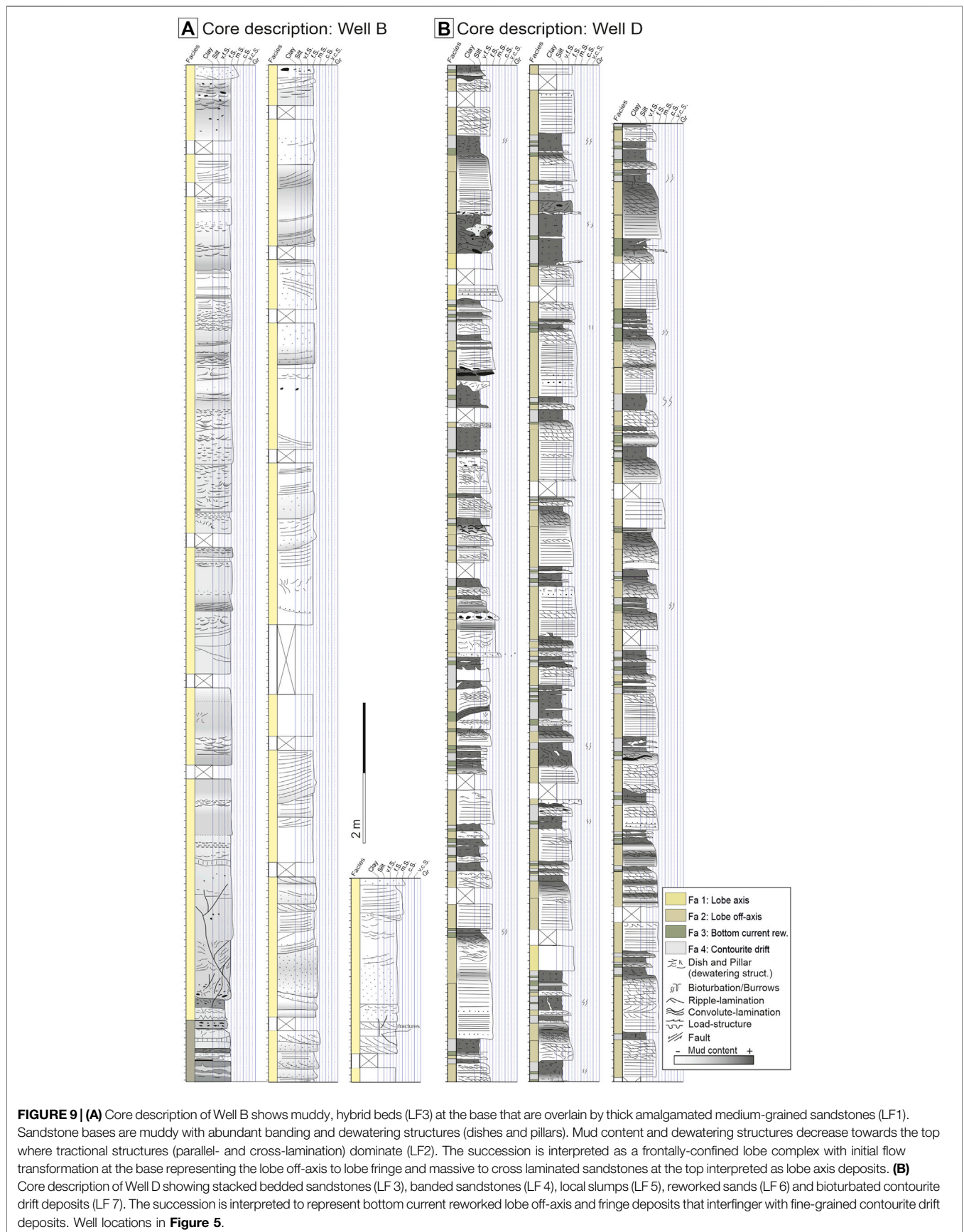


FIGURE 9 | (A) Core description of Well B shows muddy, hybrid beds (LF3) at the base that are overlain by thick amalgamated medium-grained sandstones (LF1). Sandstone bases are muddy with abundant banding and dewatering structures (dishes and pillars). Mud content and dewatering structures decrease towards the top where tractional structures (parallel- and cross-lamination) dominate (LF2). The succession is interpreted as a frontally-confined lobe complex with initial flow transformation at the base representing the lobe off-axis to lobe fringe and massive to cross laminated sandstones at the top interpreted as lobe axis deposits. **(B)** Core description of Well D showing stacked bedded sandstones (LF 3), banded sandstones (LF 4), local slumps (LF 5), reworked sands (LF 6) and bioturbated contourite drift deposits (LF 7). The succession is interpreted to represent bottom current reworked lobe off-axis and fringe deposits that interfinger with fine-grained contourite drift deposits. Well locations in **Figure 5**.

lobe off-axis and fringe facies where turbidite beds thin and drape over the gentle relief. High amplitude “fingers” extend from the south and north into a topographic low associated with the moat along the Sea Gap with amplitudes dimming away from the sediment entry points and towards the onlap surfaces (Figure 5F, Figure 7A). These elongate, laterally confined lobate bodies are about 5 km wide and 19 km long. Drift morphology flattens towards the basin low between the Sea Gap and Davie Ridge (Figure 4A). Spectral decomposition maps of the eastern 3D seismic survey show elongate northwest-southeast striking high amplitude reflectors between low amplitude, straight crested sediment waves covering the whole seismic survey (Figures 8A,D).

4.4.2 Bed-Scale Observations on Laterally Confined Lobes

Although no core data are available for the Santonian, gamma ray log responses of Well B, C and D confirm the sand-rich character of the high amplitude bodies forming the lobe complexes. Well D targets high amplitude lobe complexes in the south of the Sea Gap pop-up structure, and displays thick, blocky low gamma ray responses of about 60 m (Figure 7A, zoom I). This interval is interrupted by high gamma ray peaks in a spacing of about 20 m that are interpreted to represent individual coarse grained lobes. Well C, in the east of the Sea Gap shows a spiky log response at the base of the Santonian that correlated with the distal dimming of amplitude reflections along the distal end of the lobe complexes (Figure 7A, zoom I). Similar GR signatures are recorded in the Campanian system where core control supports the fine grained character of these lower amplitude reflections.

4.5 Campanian

4.5.1 Seismic Scale Observations on Semi-confined Lobes

The mid-Campanian reflector marks a regional unconformity (Data Rep. Table 1; green seismic horizon). Bottom current-related sedimentation ceased along the upper slope and existing topography was filled by flat, parallel, high to low amplitude reflectors interpreted as ponded turbidites (Figure 4B). Along the lower slope, east of the Sea Gap, large drift deposits continue to grow, extending further into the basin centre towards the Davie Ridge (Figures 4A,B). Mounded drifts flatten towards the basin centre into sheet-like morphologies (Figure 4A) and extensive, NNE-SSW striking sediment wave fields (wavelengths of up to 5 km) formed along the western side of the Davie Ridge (Figures 8B,E). High amplitude lobe complexes (SFA 2) fill the gentle relief of the large drift deposits in the northern and southern depocentre, east of the Sea Gap (Figures 5G–I). Seismic amplitudes indicate lobe complex sizes of up to 30 km long and 23 km wide, and dim gradually over long distances (~5 km). This transitional dimming of amplitudes suggests a low gradient and limited confinement with well-developed lobe fringe facies (Figures 7B,C). High and medium amplitude reflectors extend into the basin centre where they are confined by the topographic lows of large sediment waves (Figure 6C). Although the interpretation is hampered by the lack of 3D seismic reflection data in this area, the thickness (~300 ms [TWT]) and internal seismic facies suggest laterally confined lobe complexes in the basin centre

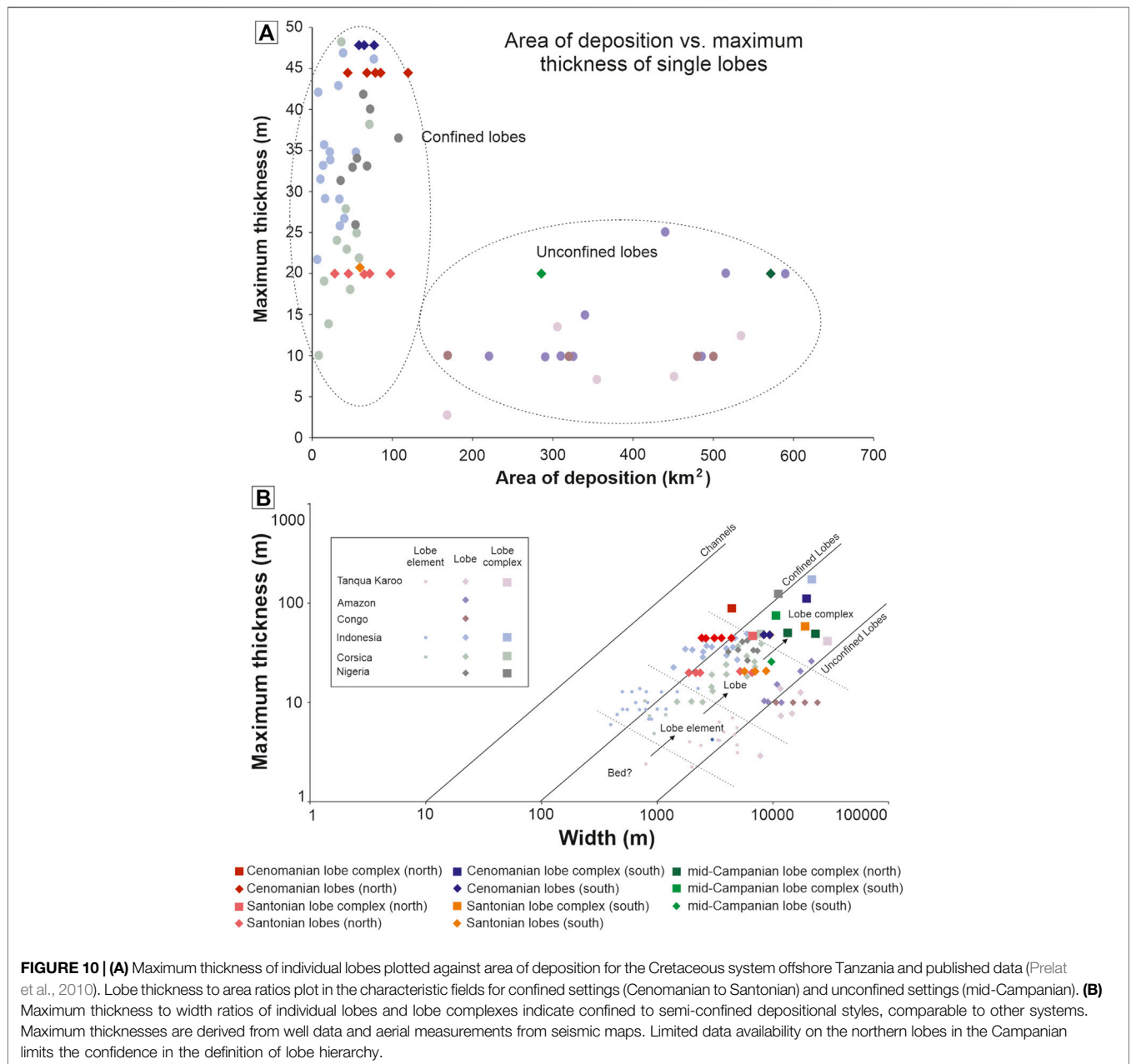
(Figure 6C)—similar to the Santonian systems. In the most distal part of the system, medium amplitude reflectors (SFA 8) onlap and drape over the crest of large sediment wave fields east of the Davie Ridge (Figures 8A,B).

4.5.2 Bed-Scale Observations on Semi-confined Lobes

Well D targets a ~75 m thick northward confined lobe complex that drapes onto the gentle relief of low amplitude drift deposits in the south of the Sea Gap (Figure 5I, Figure 7C). Spiky gamma ray signatures and ~36 m of core display a heterogeneous succession of sandstones and muddy siltstones (Figure 7C; zoom I, 9B). Medium to fine grained, normally graded sandstones up to 1.5 m thick are commonly massive to parallel- and ripple-laminated with intervals of distorted, convolute lamination (LF 3, Figure 3E). Some beds show well developed banding (LF 4, Figures 3K,L) and are often reworked by bottom currents (LF 7, Figures 3K,L). These reworked beds consist of up to fine-grained sandstone and starved ripples (often showing opposing paleo-flow indicators than the underlying beds) that are interbedded with bioturbated, fine-grained (mud- and siltstones) drift deposits (LF6, Figures 3L,M) and local debrites (LF 5, Figures 3I,J). The succession is interpreted to represent stacked lobe off-axis and lobe fringe deposits that are partly reworked by bottom currents (Fa 2 and 3) and interfinger with the toes of contourite drift deposits (Fa 4).

4.6 Scale of Bottom Current Influenced Lobe Complexes

Bottom current influenced lobe complexes have been identified along depocentres in the north and south of the Sea Gap pop-up structure in the Cenomanian, Santonian and mid-Campanian. The six lobe complexes show varying degrees of confinement by contourite drift deposits and fine grained sediment waves. Their geometric relationships are compared to other confined deep marine lobe systems described by Prélat et al. (2010) (Figure 10). Cenomanian and Santonian lobes show strong confinement with high thickness to area ratios comparable to lobes in the Kutai basin in Indonesia, Nigeria and the Golo system offshore Corsica, whereas the larger, semi-confined lobes in the mid-Campanian plot closer to unconfined systems (Figure 10A). Average dimensions of 3.5 km × 19 km × 45 m (width × length × thickness), crescentic shape, and length to width ratios of < 0.2 demonstrate the strong frontal and lateral confinement of Cenomanian and Santonian northern lobe complexes offshore Tanzania. Semi-confinement along gentle dipping large contourite drifts in the Campanian system facilitated more symmetrical lobe shapes with average dimensions of 9 km × 15 km × 47 m (width × length × thickness) and length to width ratios of ~0.4–~0.6. Limited core data and seismic resolution hampers a clear distinction between individual lobes, but average dimensions of 13 km × 25 km × 20 m (width × length × thickness) and length to width ratios of ~0.5 are inferred. Average width to thickness plots indicate comparable thickness to width ratios for bottom current influenced lobe complexes and other lobe systems as they plot along confined to semi-confined trend lines (Figure 10B). This supports the assumption that autogenic processes in gravity flows control the size and volume of individual lobes and lobe



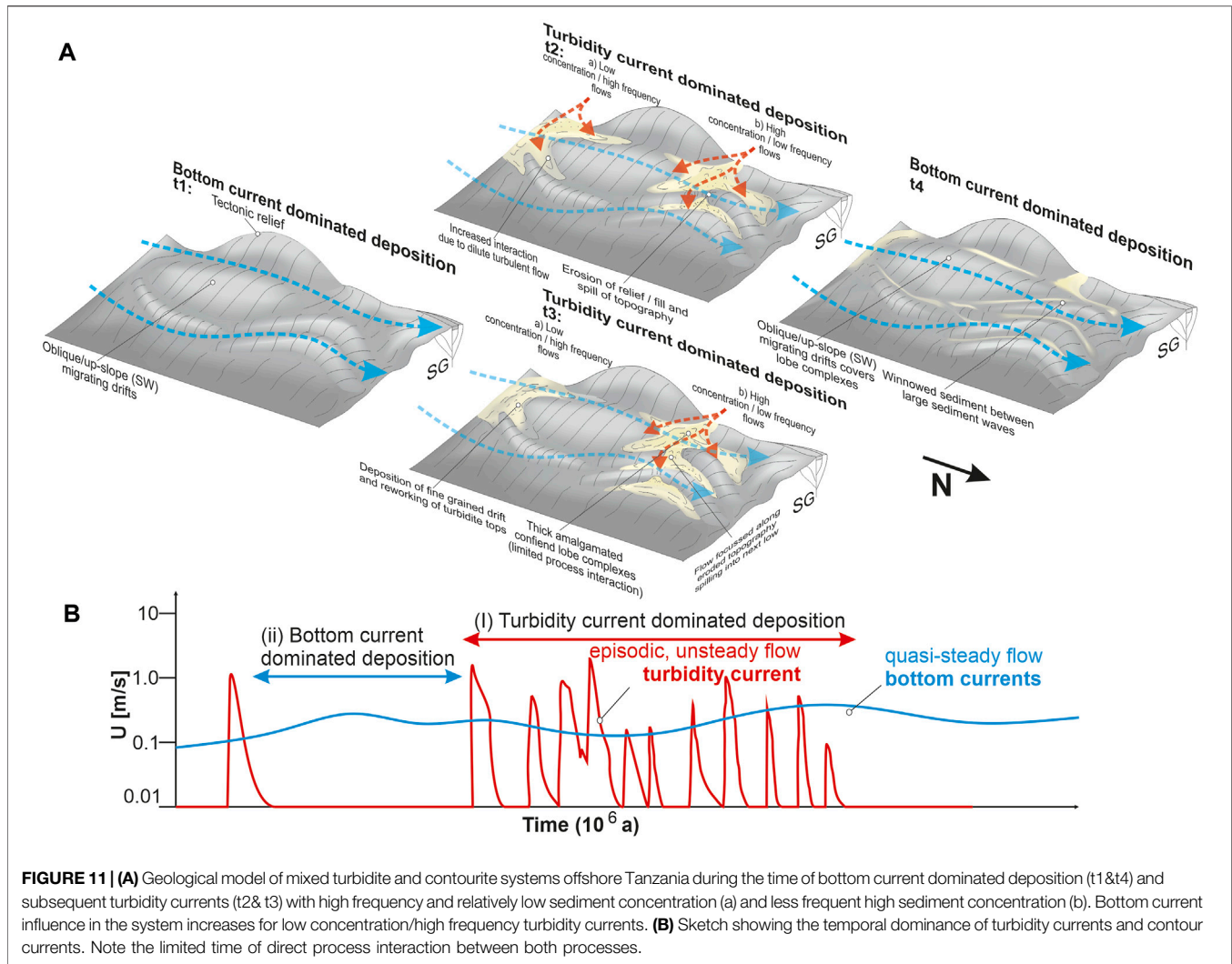
complexes (Prélat et al., 2009, 2010). The level of confinement, especially along strong lateral and frontal confined systems in the Cenomanian and Santonian leads to highly irregular, long and narrow lobes in these mixed systems.

5 DISCUSSION

5.1 Influence of Bottom Currents on Lobe Complexes

The interaction of bottom currents and sediment gravity flows is characterised by phases of: 1) “passive interaction” where sediment gravity flows and bottom currents interact with the

topography of their related deposits and 2) “active interaction” where downslope sediment gravity flows and margin parallel bottom currents interfere directly (Mulder et al., 2008). The dominance of either passive or active interaction is governed by the properties of gravity- and bottom currents in terms of velocity, sediment concentration, duration, frequency, and the angle of slope, and in which environment the two flows interact. For the Cretaceous sedimentary systems offshore Tanzania, relatively short-lived (hours to days), unsteady, sediment-laden turbidity currents are assumed to build the extensive lobe complexes (Khripounoff et al., 2003, 2009; Azpiroz-Zabala et al., 2017; Symons et al., 2017). These short-lived, sediment laden flows are superimposed on semi-continuous bottom

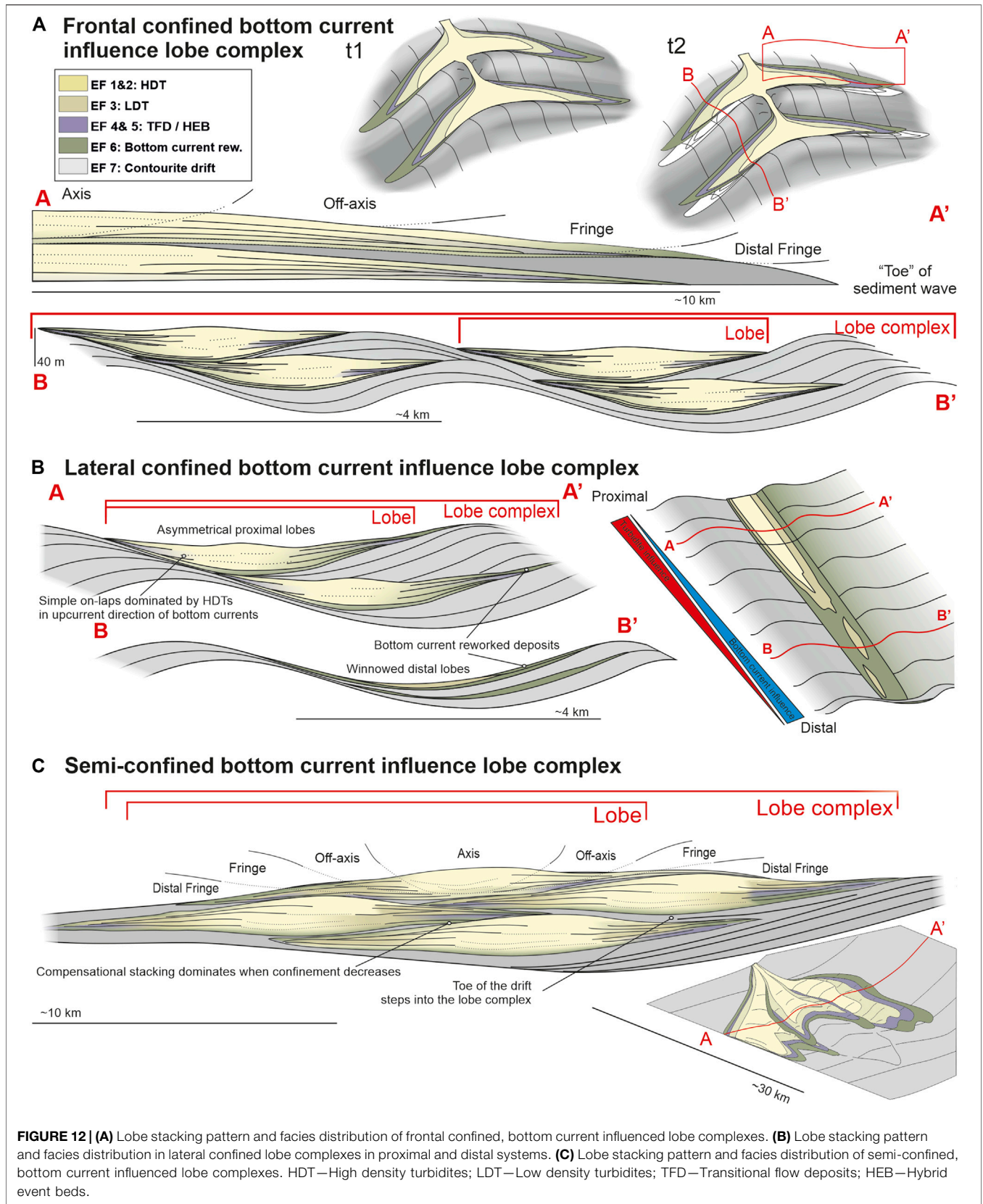


current systems that were active during the Upper Cretaceous (Fischer and Uenzelmann-Neben, 2018a; Sansom, 2018; Thiéblemont et al., 2020) (Figures 2A,B). Direct flow interaction between the two is therefore limited to the short time interval when both processes are active (Figure 11B) (Miramontes et al., 2020a; Fuhrmann et al., 2020). When bottom currents dominated the Tanzanian coastal basins in the Cretaceous, they deposited fine grained drifts and sediment waves forming complex morphologies along the lower slope and basin floor, east of the Sea Gap. These topographic features caused a variety of confinement styles for subsequent lobes that cause modification of lobe morphology, stacking pattern and facies distribution and can be distinguished as 1) frontally confined-, 2) laterally confined and 3) semi-confined bottom current influenced lobe complexes.

5.1.1 Bottom Current Dominance of the Lower Slope

During times of reduced turbidity current activity, bottom current sedimentation dominated the margin east of the Sea Gap (t1 and t4 in Figure 11). The low seismic amplitudes, morphologies and

regional extent contourite drifts and sediment waves indicate fine-grained deposits (mud- and siltstone) that were deposited by relatively persistent bottom currents (Faugères et al., 1999; Wynn and Stow, 2002a). Along the lower slope, large south-west (upstream) migrating sediment waves started to develop in the Cenomanian that are aligned with the contours of the tectonic relief of the Sea Gap and show an overall northwest-southeast orientation in the basin centre. Their basin-wide extent indicates a deposition by the extension of intermediate waters that flowed northwards into the Mozambique Channel and East African Basins offshore Tanzania (Figure 2) (Fischer and Uenzelmann-Neben, 2018a; Thiéblemont et al., 2020). Sediment wave size, orientation and fine-grained character suggest deposition under lee-wave conditions by relatively weak bottom currents ($0.15\text{--}0.25\text{ m}^*\text{s}^{-1}$) (Flood, 1988; Flood and Shor, 1988; Stow et al., 2009). The relatively weak bottom currents travelled over gentle relief and deposited fine-grained (up to silt sized) sediment on the lee-side of sediment waves and thus the waves migrated in, or oblique to the up-current direction (Flood, 1988; Flood and Shor, 1988). Local variations in sediment wave shape, such as the crescent shaped wave crests in



the Cenomanian may be caused by the ongoing growth of the large pop-up structure on the Sea Gap or flow interference with local dilute turbidity currents. However, the northwest to southeast striking trend of sediment waves continues throughout the Turonian to Santonian as distal as the Davie Ridge (**Figure 8**). This supports regionally constant northwards flowing currents that increased in strength during the Cretaceous Thermal Maximum Event in the Turonian (Poulsen et al., 2001, 2003; Friedrich et al., 2012; Murphy and Thomas, 2012). Larger drift deposits of the Cenomanian to mid-Campanian nucleated along the growing tectonic relief of the Sea Gap with moats and mixed turbidite-contourite channel complexes dominating the upper slope. Contourite drifts along the lower slope flatten towards the basin centre and transition into sediment wave fields along the Davie Ridge. The sediment incorporated in the extensive contourite depositional system is likely sourced from the south where northward-flowing bottom currents caused erosion, and limited drift deposition during the Upper Cretaceous (Fischer and Uenzelmann-Neben, 2018a; Thiéblemont et al., 2020). Additional fines could have been stripped from local turbidity currents (Fossum et al., 2019), local erosion events (Hollister and McCave, 1984; McCave and Tucholke, 1986; McCave et al., 2017; Thran et al., 2018) or from paleo-Rovuma River in the south (Key et al., 2008; Smelror et al., 2008). During the mid-Campanian, bottom current sedimentation ceased along the upper slope and sediment wave orientation along the Davie Ridge changed from SSE-NNW to NNE-SSW. Time equivalent onset of bottom current related sedimentation along the Mozambique Channel and Mozambique ridge indicates a change in the palaeo-oceanographic setting that was likely caused by a deepening of the Aghulas Passage and re-orientation of major currents (**Figures 2A,B**) (Fischer and Uenzelmann-Neben, 2018a; Thiéblemont et al., 2020). This variability in bottom current sedimentation in the Upper Cretaceous caused the evolution of complex margin topography and the deposition of distinctive turbidite lobe complexes.

5.1.2 Frontally-Confining Lobe Complexes

Frontally-confined lobe complexes developed dominantly in the Cenomanian, in the northern depocentre, where transverse sediment gravity flows filled topographic lows between crescent-shaped sediment waves (**Figure 11 t2b, Figure 12A**). Channelised, high amplitude reflectors are interpreted as sediment entry points into each topographic low, indicating filling of topography in a fill-and-spill fashion, similar to steeply confined mini-basins (Prather et al., 2012, 2016) or other small scale sea-floor bedforms (Maselli et al., 2019). These confined structures are dominated by aggradational lobe stacking and distinct phases of flow ponding, flow stripping and bypass (Sinclair and Tomasso, 2002). Core data in Well B represents the progressive infill of such a steeply confined structure. Initial flows that become confined rapidly decelerate along the frontal confinement leading to the development of muddy, hybrid beds and slumps (Lf 2 and 4) that represent lobe off-axis to proximal fringe deposits along onlap surfaces (Fa. 2) (**Figure 2B**) (Al Ja'Aidi et al., 2004; Haughton et al., 2009; Bakke et al., 2013; Patacci et al., 2014, 2015; Soutter et al., 2019). With ongoing

sediment progradation, highly concentrated turbidity currents enter the confined structure and decelerate along the frontal confinement, which causes frontal erosion and rapid deposition of massive amalgamated high-density turbidites, and entrainment of a wide grain size range (Lf 1) (Lowe, 1982; Soutter et al., 2021). This rapid deposition and large grain-size range promotes the trapping of pore waters along low permeability laminae that eventually burst with increasing fluid pressure, and form the well-developed banding and dewatering structures (dishes and pillars) (Lowe, 1975; Porten et al., 2019). Ongoing infill and erosion along the frontal confinement allows sediment-laden flows to bypass into the next topographic low (**Figure 11 t3b**). With increasing sediment bypass, high-density turbidites are dominantly deposited by continuous deposition, which is represented by a decrease in dewatering structures and the increase in steepening cross bedding (Lf 2) (**Figure 3C, Figure 9A**) (Hiscott, 1994; Kneller and Branney, 1995). The steepening cross bedding in the upper part of the core may be associated with long sediment waves or the backfilling of large scours in the proximal location of the lobe axis (Fa 1) (Arnott and Al-Mufti, 2017; Pohl et al., 2019). Increased flow velocities are associated with narrow erosional corridors through which flows are focussed and accelerated (Soutter et al., 2021), that support locations of sustained sediment bypass (Amy et al., 2000; Stevenson et al., 2015). The lack of bottom current influence on axial lobe deposits is interpreted to result from strong confinement and high sediment concentration of the gravity currents in which grain-grain interaction in the high density layer at the base of the flow dominate the transport over dilute turbulent flow (Lowe, 1982; Talling et al., 2012). Bottom current influence in these low velocity bottom current systems ($0.1\text{--}0.3\text{ m}\cdot\text{s}^{-1}$) is inferred to be pronounced along the fine grained lobe fringe where dilute, super-elevated cloud of turbidity currents strip away or locally re-distribute finer grains in the down-current direction (in respect to the bottom current) (*sensu de Castro et al., 2020*). High sediment concentration and long recurrence times of turbidity currents at terminal lobes (Jobe et al., 2018) in combination with steep contourite relief may favour a passive interaction of these processes-similar to other confined systems (**Figure 12**). During times of long quiescence (of turbidity currents), sediment waves migrate southwest and cause a re-routing of sediment gravity flows and a modification of lobe complex stacking pattern (**Figure 11 t4**).

5.1.3 Laterally Confined Lobe Complexes

Lateral confinement is observed in the Santonian along the Sea Gap and the mid-Campanian in the west of the Davie Ridge, where sediment gravity flows are confined along straight-crested sediment waves. Core was not recovered, but high seismic amplitudes and gamma ray log data from Well B (similar to the responses along cored sections) indicate coarse-grained sediments in the topographic lows between the sediment waves (**Figure 5, Figure 7, Figure 8**). Sediment is inferred to have been sourced from the northwest and entered the confinement axially. This

lateral confinement increases the run out length of turbidity currents and the deposition of elongated lobes (Salles et al., 2014; Soutter et al., 2021). Asymmetrical draping of high amplitude bodies out of the confinement and dimming of amplitudes towards the northeast suggest an increasingly active interaction of bottom currents with confined turbidity currents similar to “mixed” contourite-turbidite channels (Fuhrmann et al., 2020; Miramontes et al., 2020b). Flow stripping and reworking by bottom currents causes a facies asymmetry and the deposition of bottom current reworked sands (Fa 3) on the down current side of the sediment waves in respect to the bottom current similar to other systems (Shanmugam et al., 1993; de Castro et al., 2020; Fonnesu et al., 2020) (**Figure 12B**). Away from the sediment entry point the turbidity currents wane, grain size decreases (represented by the dimming of seismic amplitudes) and bottom-current influence increases. During the shutdown of turbidity currents, margin-parallel bottom currents, acted with an angle of up to 45° (in respect to the elongated deposit), reworked and deposited fined-grained material on the bottom current upstream facing side of the sediment waves (Hopfauf and Spieß, 2001; Wynn and Stow, 2002b). This interplay of processes suggests a stacking of fine grained drift deposits (Fa 4) and reworked lobe fringe deposits (Fa 3) on the up-current facing side of the sediment waves and coarse grained turbidite facies (Fa 1 and 2) in the centre of the structure. With increasing distance from the margin, bottom currents dominate and facies ratios changes towards drift deposits and bottom current reworked deposits (Fa 4 and Fa 5). This transition is seen along the Davie Ridge in the Cenomanian to mid-Campanian where large sediment-wave fields show dim amplitudes along topographic lows that are draped towards the northern wave crests (**Figure 8**).

5.1.4 Semi-confined Lobe Complexes

Semi-confined lobes are present along the southern depo-centre in the Cenomanian, Santonian and the mid-Campanian. Deposits are of elongated, lobate shape with high seismic amplitudes that dim towards the fringes where they onlap and drape over low angle contourite drifts (**Figure 11**, **Figure 12C**). Individual architectural elements across lobe complex are well developed in form of ~300 m wide distributary channel-fills in proximal location, and individual lobes with high-amplitude reflections in the axis that dim towards the fringes (**Figure 5I**, **Figure 7B,C**). Amplitude dimming is interpreted to represent well preserved lobe off-axis and fringe deposits developed due to longer flow runouts along the gentle relief (e.g., Hansen et al., 2019; Spychala et al., 2017). Lateral, one sided confinement dominates the lobes along the margins of fine grained, low-angle drift deposits, causing draping onlaps and aggradation, with lateral accretion and compensational stacking observed towards the unconfined flank similar to other systems (Gervais et al., 2006; Deptuck et al., 2008; Hansen et al., 2019). Core data of Well D reveals complex facies stacking along the lobe off-axis and lobe fringes (**Figure 9B**). Increased flow run-out lengths along and onto the gentle relief allow grain size segregation and well developed, normally-graded turbidite beds (LF 3) that thin away from the

focal point and are commonly associated with lobe fringes (Spychala et al., 2017). The locally well-developed banding in individual beds (LF 4) is interpreted to result from transitional flows (switching from turbulent to laminar flows) (Baas et al., 2009; Sumner et al., 2009). Flow transformation was likely caused by the entrainment of mud due to local erosion of muddy contourite drifts and the interaction with local topography (Kneller et al., 1991; Kane and Pontén, 2012). Further indicators for local influence of topography are convolute lamination (Tinterri et al., 2016), slumped deposits and sand injectites that result from remobilisation of unconsolidated sediment along the depositional relief and the build-up of overpressure during burial of sandstones along onlaps (Cobain et al., 2017; Hansen et al., 2019). This topographic complexity may have also caused opposing palaeo-current indicators in form of ripple lamination within individual beds (Bell et al., 2018b).

Additional complexity to the facies stacking is interpreted to result from the influence of bottom currents along the lower slope of the Upper Cretaceous sedimentary systems (**Figures 2A,B**) (Fischer and Uenzelmann-Neben, 2018a; Thiéblemont et al., 2020). Interbedded starved ripples and streaks of fine-grained sandstone and muddy siltstones that consistently overlie turbidite beds are interpreted to represent reworking by bottom currents (Fa 3) (Ito, 1996; de Castro et al., 2020). The paleocurrent indicators of these laminae differ from the underlying beds, which may either be the result of flow deflection or lateral reworking of bottom currents (**Figure 3K**; white arrow) (Shanmugam et al., 1993; Martin-Chivelet et al., 2008; de Castro et al., 2020). The regional context and re-occurrence of these beds favour a reworking by temporally variable bottom currents with local velocities of up to $0.3 \text{ m} \cdot \text{s}^{-1}$ (Stow et al., 2009 and references therein) (**Figure 11t2 to t3**). The thick, mottled, muddy siltstones, with faint, up to fine-grained sandstone lenses and streaks (**Figure 3I**, Fa 5) are interpreted as toes of the drift deposits that migrate onto the turbidite lobes during the absence of turbidity currents (Fa 4) (**Figure 11t4**). Increased run-out lengths along gentle topography and frequency of turbidity currents control the facies-stacking pattern. Higher sedimentation rates along the proximal lobe fringes promotes the preservation of individual tractional sedimentary structures (Fa3) that are increasingly disrupted by bioturbation towards the most distal parts of the system. These mottled and poorly sorted siltstones resemble commonly described contourite drift facies (Fa 4) (Stow et al., 2008; Stow and Faugères, 2008; Brackenridge et al., 2013).

5.2 Global Variability of the Evolution of Bottom Current Influenced Lobes

This study shows how the temporal interaction of turbidity- and contour currents influenced the deposition, facies and stacking patterns of submarine lobe complexes offshore Tanzania. The system is characterised by strong turbidity currents, tectonic relief along large transform faults and relatively slow bottom

current velocities ($0.1\text{--}0.30\text{ m}\cdot\text{s}^{-1}$) that form sediment waves and large contourite drifts. However, other deep-marine sedimentary systems vary greatly in terms sediment supply rates, bottom current velocity and variability or the frequency of turbidity currents and margin morphology. Turbidity currents are mainly controlled by external controls including climate, tectonics and sea-level that govern the size of the catchment, length of the system, and ultimately the sediment supply rate (Covault and Graham, 2010; Sømme et al., 2011; Romans et al., 2016; Hessler and Fildani, 2019). Bottom currents are similarly variable in terms of their velocity, and sediment transport capacity along a margin depending on global climate conditions, ocean connectivity and sea-floor topography (Hollister and McCave, 1984; Faugères and Mulder, 2011; Gardner et al., 2017; Thran et al., 2018). Margin morphology and local velocity variations have a strong influence on bottom current systems and in turn mixed-turbidite-contourite systems (Miramontes et al., 2021). Examples of bottom current influenced passive margin morphologies are the modern systems offshore Uruguay and Argentina where velocity differences and internal processes along pycnoclines form extensive contourite terraces (Preu et al., 2013; Hernández-Molina et al., 2016a). Tectonically active margins such as the Upper Cretaceous transform margin offshore Tanzania (this study), the Hikurangi accretion wedge or the enclosed Mediterranean Sea are associated with localised current cores that form a complex pattern of erosion and deposition (Hernández-Molina et al., 2008; García et al., 2009; Ercilla et al., 2016; Bailey et al., 2020). To generalise one can differentiate between high and low velocity bottom current systems, although there may be strong local variability around topographic obstacles or narrow straits.

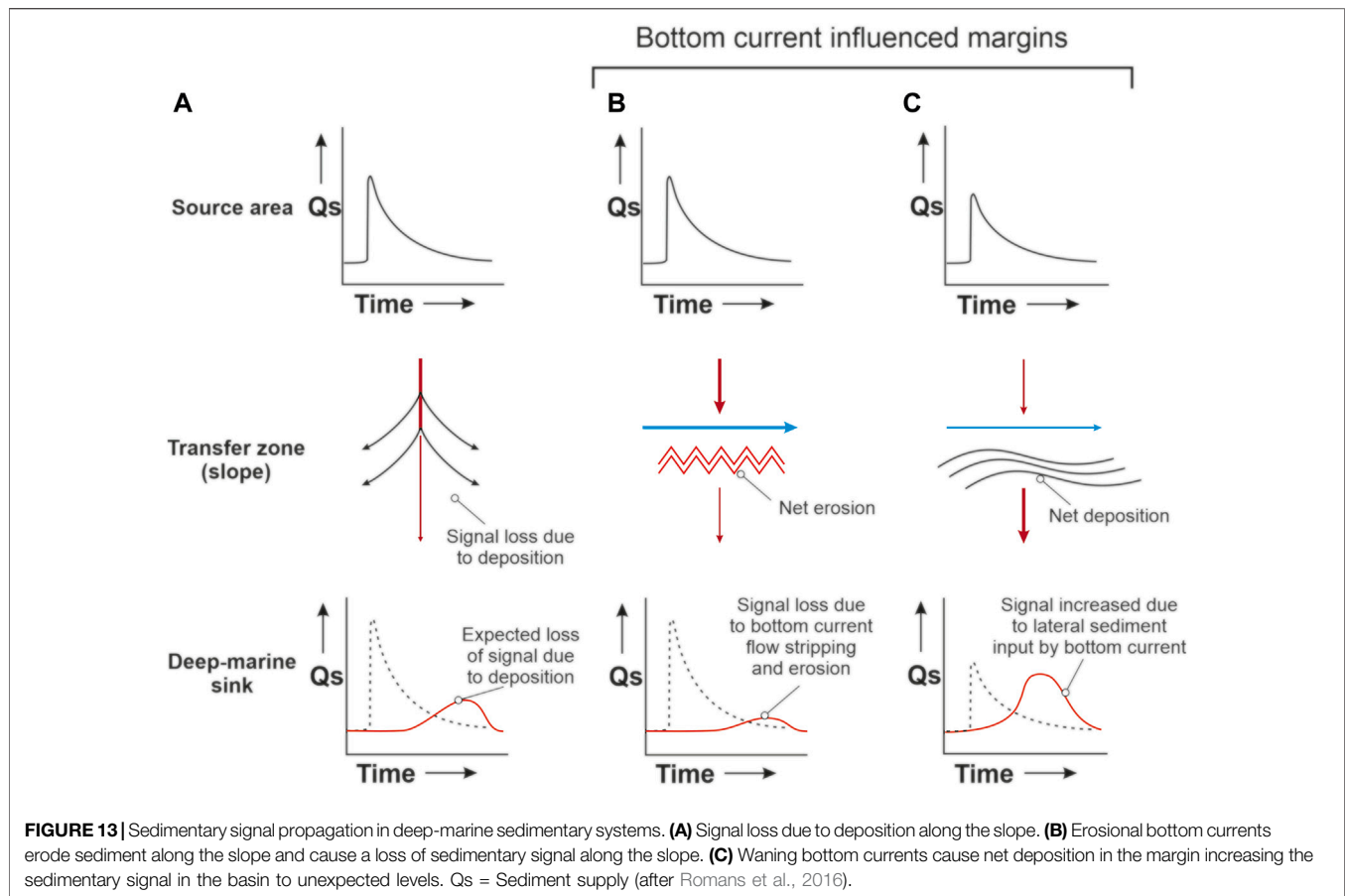
Relatively low velocity, depositional contourite systems with current velocities around $\sim 0.1\text{--}0.3\text{ m}\cdot\text{s}^{-1}$ deposit large, fine grained drifts or sediment waves, depending on the local slope angle topography, and supply of fine-grained material (Faugères et al., 1999). When large, sediment laden, depositional turbidity currents interact with these systems, direct flow interaction between bottom currents and turbidity currents is limited to the dilute upper cloud of the turbidity current and the sedimentary signal is only preserved in the fine grained lobe fringes. Lobe morphology and facies distribution along these systems is therefore controlled by the passive interaction of turbidity currents with the contourite depositional relief: frontal-, lateral- and semi- or asymmetrical (Figures 11, 12). Lobe connectivity and stacking patterns therefore depend on the frequency of turbidity currents and changes in contourite drift morphology during their absence (Marchès et al., 2010). Rare, large turbidity currents that feed the base of slope systems (Jobe et al., 2018) along high relief systems are inferred to deposit thick amalgamated sandstones between contourite drifts, similar to other steep-sided mini-basins, as in the Cenomanian case study (Figure 12A). Smaller, intra slope lobes that receive less voluminous flows at a higher frequency (Jobe et al., 2018) tend to lead to interbedded turbidite and contourite facies that show a higher degree of bottom current reworking equivalent to the facies stacking of the mid-

Campanian of this study and other locations (de Castro et al., 2020) (Figures 12B,C).

Strong bottom current systems on the other hand have been shown to be able to rework sands, forming gravel lags and barchan dunes at velocities of about $0.5\text{--}1.5\text{ m}\cdot\text{s}^{-1}$ (Masson et al., 2004; Stow et al., 2009). These sedimentary structures occur on several contourite terraces and base of slope systems where currents are constricted (Habgood et al., 2003; Masson et al., 2004; Wynn and Masson, 2008; Hernández-Molina et al., 2017). Where strong currents interact with turbidite lobes they may partly rework and strip away the fine-grained fraction in the down-current direction (of the bottom current) and form large associated fan drift deposits such as the Hikurangi fan drift along the southwest margin of New Zealand (Lewis, 1994; Carter and McCave, 2002), and NW America margin (Locker and Laine, 1992). The removal of fines by direct flow stripping and sediment reworking may winnow the sandstones and enhance reservoir quality in these mixed turbidite-contourite lobes (Fonnesu et al., 2020). When current velocities increase further, extensive reworking of turbidite lobes may form barchan dune fields and sand sheets of well sorted, fine grained sandstone as it the case in Upper Cretaceous and Tertiary systems offshore Brazil (Mutti et al., 2014). Along these high velocity systems substantial amounts of fine-grained sediment are inferred to be transported laterally along the slope and deposit where bottom currents wane along the margin.

5.3 Sediment Distribution Along Bottom Current Influenced Margins

The variability of bottom current systems and their potential to capture and redistribute sediment along continental slopes is not accounted for in source to sink models. Large scale sediment distribution in a deep-marine sedimentary basin is controlled by the external sediment supply (Qs) that is governed by climate, tectonic uplift, and eustatic sea-level changes (Sømme et al., 2009, 2011; Covault and Graham, 2010). The sedimentary signal, i.e., the rate at which sediment is produced, transported or deposited, is then modified along the transfer zone by deposition, temporal storage or lateral sediment transport before it reaches the deep-water sink (Figure 13A) (Castelltort and Van Den Driessche, 2003; Romans et al., 2016). Under conditions of high velocity bottom currents ($>0.5\text{ m}\cdot\text{s}^{-1}$) the system encounters local net erosion and the sedimentary signal received in the distal end of the system decreases (Figure 13B). Where bottom currents wane in the down-current direction sediment deposition increases, thus lifting the sedimentary signal above expected values based on the local source area (Figure 13C). This lateral sediment transport may starve certain areas of fine grained sediment and cause the development of extensive contourite drift systems in others. One such example may have been the East African Margin in the Upper Cretaceous where continuous northward flowing currents are inferred to have transported vast amounts of fine-grained sediments from



the Mozambique Margin to the north where they, contributed to extensive fine-grained drift deposits offshore Tanzania (Sansom, 2018; Thiéblemont et al., 2020; this study).

High velocity systems indicate similar along-slope transport of sediment by bottom currents along contourite terraces offshore Uruguay and Argentina (Preu et al., 2012, 2013; Hernández-Molina et al., 2016a, 2017), base of slope systems offshore Brazil (Mutti et al., 2014), the North Atlantic (Campbell and Mosher, 2016), the Faroe-Shetland and Faroe Bank Channels (Masson et al., 2004) and the Gulf of Cadiz (Habgood et al., 2003; Hernández-Molina et al., 2016b). The strong along-slope transport of sediment on contourite terraces may persist over vast distances before bottom currents wane or the core of a bottom current is caught by steeply incised canyons and diverted downslope (Marchès et al., 2007; Preu et al., 2012; Amundsen et al., 2015; Warratz et al., 2019). Thus terminal lobe complexes at the base of slope may be disconnected from their sediment source and complicate the reconstruction of sediment budgets and the stratigraphic evolution of a margin. Temporal variability of this lateral transport may further enhance complexity of these mixed systems as is shown along the Uruguay margin. Here sea-level changes caused a shift of the pycnocline and a switch a sedimentary system towards deposition of fine grained sediment waves and passive ponding of turbidite lobes, similar to the systems

described in this study (Hernández-Molina et al., 2017). These examples show the complexity of mixed-turbidite-contourite systems and the importance to further study these systems to correctly interpret the evolution of continental margins.

6 CONCLUSION

The influence of margin parallel bottom currents on Upper Cretaceous deep-marine lobe complexes offshore Tanzania is documented. It is shown that these systems are controlled by the different flow characteristics of turbidity currents and margin parallel bottom currents (e.g., duration, frequency, velocity, concentration, and angle with respect to slope) and the time during which both mechanisms are active. Contourite related relief, such as fine grained sediment waves and large drift deposits deposited by relatively weak bottom currents ($10\text{--}30\text{ cm}^2\text{s}^{-1}$), confine individual lobes and control their morphology and stacking patterns, which can be classified as: 1) frontally confined, 2) laterally confined and 3) semi-confined. Facies distributions reflect these confinement styles and flow characteristics of both turbidity- and bottom currents with thick amalgamated sandstones in the lobe axis, and increased amounts of flow transformation towards confining relief. The preservation of bottom current related facies is limited to the lobe fringes where

dilute turbidity currents carry fine grained sediment that are prone for bottom current reworking. Globally these systems vary greatly as ocean circulation and local effects, such as narrow seaways, may increase bottom current velocity and cause complete or partial erosion of deep-marine lobes. Increased lateral sediment transport may alter the sediment availability along continental margins and influence the balance of source to sink models along bottom current influenced margins.

DATA AVAILABILITY STATEMENT

The datasets presented in this article are not readily available because; Seismic and core data are owned by Equinor ASA.

AUTHOR CONTRIBUTIONS

AF analysed and processed most of the data, and wrote the manuscript. AF, IK, ES, and MC collected and interpreted the data. AF, AP, IK designed the figures. All authors contributed to the manuscript.

REFERENCES

- Al Ja'Aidi, O. S., McCaffrey, W. D., and Kneller, B. C. (2004). Factors Influencing the deposit Geometry of Experimental Turbidity Currents: Implications for Sand-Body Architecture in Confined Basins. *Geol. Soc. Lond. Spec. Publications* 222, 45–58. doi:10.1144/GSL.SP.2004.222.01.04
- Amundsen, H. B., Laberg, J. S., Vorren, T. O., Hafliðason, H., Forwick, M., and Buhl-Mortensen, P. (2015). Late Weichselian-Holocene Evolution of the High-Latitude Andøya Submarine Canyon, North-Norwegian continental Margin. *Mar. Geology* 363, 1–14. doi:10.1016/j.margeo.2015.02.002
- Amy, L., Kneller, B., and McCaffrey, W. (2000). Evaluating the Links between Turbidite Characteristics and Gross System Architecture: Upscaling Insights from the Turbidite Sheet-System of Peira Cava, SE France. *Deep. Reserv. World 20th Annu.*, 1–15. doi:10.5724/gcs.00.15.0001
- Armitage, D. A., Romans, B. W., Covault, J. A., and Graham, S. A. (2009). The Influence Of Mass-Transport-Deposit Surface Topography On The Evolution Of Turbidite Architecture: The Sierra Contreras, Tres Pasos Formation (Cretaceous), Southern Chile. *J. Sedimen. Res.* 79 (5), 287–301. doi:10.2110/jsr.2009.035
- Arnott, R. W. C., and Al-Mufti, O. (2017). Deep-Marine Pseudo Dune Cross-Stratification-Similar, but Completely Different. *J. Sediment. Res.* 87, 312–323. doi:10.2110/jsr.2017.21
- Azpiroz-Zabala, M., Cartigny, M. J. B., Talling, P. J., Parsons, D. R., Sumner, E. J., Clare, M. A., et al. (2017). Newly Recognized Turbidity Current Structure Can Explain Prolonged flushing of Submarine Canyons. *Sci. Adv.* 3, e1700200. doi:10.1126/sciadv.1700200
- Baas, J. H., Best, J. L., and Peakall, J. (2011). Depositional Processes, Bedform Development and Hybrid Bed Formation in Rapidly Decelerated Cohesive (Mud-sand) Sediment Flows. *Sedimentology* 58, 1953–1987. doi:10.1111/j.1365-3091.2011.01247.x
- Baas, J. H., Best, J. L., Peakall, J., and Wang, M. (2009). A Phase Diagram for Turbulent, Transitional, and Laminar Clay Suspension Flows. *J. Sediment. Res.* 79, 162–183. doi:10.2110/jsr.2009.025
- Bailey, W. S., McArthur, A. D., and McCaffrey, W. D. (2020). Distribution of Contourite Drifts on Convergent Margins: Examples from the Hikurangi Subduction Margin of New Zealand. *Sedimentology* 68, 294–323. doi:10.1111/sed.12779
- Bakke, K., Kane, I. A., Martinsen, O. J., Petersen, S. A., Johansen, T. A., Hustoft, S., et al. (2013). Seismic Modeling in the Analysis of Deep-Water sandstone Termination Styles. *Bulletin* 97, 1395–1419. doi:10.1306/03041312069

FUNDING

This work was funded by Equinor ASA. MC was supported by the Climate Linked Atlantic Sector Science (CLASS) program (Natural Environment Research Council Grant No. NE/R015953/1).

ACKNOWLEDGMENTS

We thank David M. Hodgson for his comments on the early version of this manuscript. Naohisa Nishida and Maarten Van Daele are thanked for their constructive reviews that helped to further improve the manuscript. We are grateful to Equinor ASA for funding this research and providing the data.

SUPPLEMENTARY MATERIAL

The Supplementary Material for this article can be found online at: <https://www.frontiersin.org/articles/10.3389/feart.2021.752066/full#supplementary-material>

- Barker, S. P., Haughton, P. D., McCaffrey, W. D., Archer, S. G., and Hakes, B. (2008). Development Of Rheological Heterogeneity In Clay-Rich High-Density Turbidity Currents: Aptian Britannia Sandstone Member, UK Continental Shelf. *J. Sedimen. Res.* 78 (2), 45–68. doi:10.2110/jsr.2008.014
- Bell, D., Kane, I. A., Pontén, A. S. M., Flint, S. S., Hodgson, D. M., and Barrett, B. J. (2018a). Spatial Variability in Depositional Reservoir Quality of Deep-Water Channel-Fill and Lobe Deposits. *Mar. Pet. Geology* 98, 97–115. doi:10.1016/j.marpetgeo.2018.07.023
- Bell, D., Stevenson, C. J., Kane, I. A., Hodgson, D. M., and Poyatos-Moré, M. (2018b). Topographic Controls on the Development of Contemporaneous but Contrasting Basin-Floor Depositional Architectures. *J. Sediment. Res.* 88, 1166–1189. doi:10.2110/jsr.2018.58
- Best, J., and Bridge, J. (1992). The Morphology and Dynamics of Low Amplitude Bedwaves upon Upper Stage Plane Beds and the Preservation of Planar Laminae. *Sedimentology* 39, 737–752. doi:10.1111/j.1365-3091.1992.tb02150.x
- Brackenkridge, R. E., Hernández-Molina, F. J., Stow, D. A. V., and Llave, E. (2013). A Pliocene Mixed Contourite-Turbidite System Offshore the Algarve Margin, Gulf of Cadiz: Seismic Response, Margin Evolution and Reservoir Implications. *Mar. Pet. Geology* 46, 36–50. doi:10.1016/j.marpetgeo.2013.05.015
- Brackenkridge, R. E., Stow, D. A. V., Hernández-Molina, F. J., Jones, C., Mena, A., Alejo, I., et al. (2018). Textural Characteristics and Facies of Sand-Rich Contourite Depositional Systems. *Sedimentology* 65, 2223–2252. doi:10.1111/sed.12463
- Bull, S., Cartwright, J., and Huuse, M. (2009). A Review Of Kinematic Indicators From Mass-Transport Complexes Using 3D Seismic Data. *Marine Petrol. Geol.* 26 (7), 1132–1151. doi:10.1016/j.marpetgeo.2008.09.011
- Bouma, A. (1964). *Turbidites. In Developments in sedimentology* Elsevier 3, 247–256.
- Calvin Campbell, D., and Mosher, D. C. (2016). Geophysical Evidence for Widespread Cenozoic Bottom Current Activity from the continental Margin of Nova Scotia, Canada. *Mar. Geology* 378, 237–260. doi:10.1016/j.margeo.2015.10.005
- Carter, L., and McCave, I. N. (2002). Eastern New Zealand Drifts, Miocene-Recent. *Geol. Soc. Lond. Mem.* 22, 385–407. doi:10.1144/GSL.MEM.2002.022.01.27
- Castelino, J. A., Eagles, G., and Jokat, W. (2016). Anomalous Bathymetry and Palaeobathymetric Models of the Mozambique Basin and Riiser Larsen Sea. *Earth Planet. Sci. Lett.* 455, 25–37. doi:10.1016/j.epsl.2016.09.018
- Castelltort, S., and Van Den Driessche, J. (2003). How Plausible Are High-Frequency Sediment Supply-Driven Cycles in the Stratigraphic Record? *Sediment. Geology* 157, 3–13. doi:10.1016/S0037-0738(03)00066-6

- Clift, P. D., Shimizu, N., Layne, G. D., Blusztajn, J. S., Gaedicke, C., Schlüter, H.-U., et al. (2001). Development of the Indus Fan and its Significance for the Erosional History of the Western Himalaya and Karakoram. *Bull. Geol. Soc. Am.* 113, 1039–1051. doi:10.1130/0016-7606(2001)113<1039:dotifa>2.0.co;2
- Cobain, S. L., Hodgson, D. M., Peakall, J., and Shiers, M. N. (2017). An Integrated Model of Clastic Injectites and basin Floor Lobe Complexes: Implications for Stratigraphic Trap Plays. *Basin Res.* 29, 816–835. doi:10.1111/bre.12229
- Covault, J. A., and Graham, S. A. (2010). Submarine Fans at All Sea-Level Stands: Tectono-Morphologic and Climatic Controls on Terrigenous Sediment Delivery to the Deep Sea. *Geology* 38, 939–942. doi:10.1130/G31081.1
- Cumberpatch, Z. A., Kane, I. A., Soutter, E. L., Hodgson, D. M., Jackson, C. A.-L., Kilhams, B. A., et al. (2021). Interactions between Deep-Water Gravity Flows and Active Salt Tectonics. *J. Sediment. Res.* 91, 34–65. doi:10.2110/jsr.2020.047
- de Castro, S., Hernández-Molina, F. J., Rodríguez-Tovar, F. J., Llave, E., Ng, Z. L., Nishida, N., et al. (2020). Contourites and Bottom Current Reworked Sands: Bed Facies Model and Implications. *Mar. Geology*. 428, 106267. doi:10.1016/j.margeo.2020.106267
- Deptuck, M. E., Piper, D. J. W., Savoye, B., and Gervais, A. (2008). Dimensions and Architecture of Late Pleistocene Submarine Lobes off the Northern Margin of East Corsica. *Sedimentology* 55, 869–898. doi:10.1111/j.1365-3091.2007.00926.x
- Donnadieu, Y., Pucéat, E., Moiroud, M., Guillocheau, F., and Deconinck, J. F. (2016). A Better-Ventilated Ocean Triggered by Late Cretaceous Changes in continental Configuration. *Nat. Commun.* 7. doi:10.1038/ncomms10316
- Doughty-Jones, G., Mayall, M., and Loneragan, L. (2017). Stratigraphy, Facies, and Evolution of Deep-Water Lobe Complexes within a Salt-Controlled Intraslope Minibasins. *Bulletin* 101, 1879–1904. doi:10.1306/01111716046
- Ercilla, G., Juan, C., Hernández-Molina, F. J., Bruno, M., Estrada, F., Alonso, B., et al. (2016). Significance of Bottom Currents in Deep-Sea Morphodynamics: An Example from the Alboran Sea. *Mar. Geology*. 378, 157–170. doi:10.1016/j.margeo.2015.09.007
- Faugères, J.-C., and Mulder, T. (2011). Contour Currents and Contourite Drifts. *Dev. Sedimentol.* 63, 149–214. doi:10.1016/B978-0-444-53000-4.00003-2
- Faugères, J.-C., Stow, D. A. V., Imbert, P., and Viana, A. (1999). Seismic Features Diagnostic of Contourite Drifts. *Mar. Geology*. 162, 1–38. doi:10.1016/S0025-3227(99)00068-7
- Ferguson, R. A., Kane, I. A., Eggenhuisen, J. T., Pohl, F., Tilston, M., Sychala, Y. T., et al. (2020). Entangled External and Internal Controls on Submarine Fan Evolution: an Experimental Perspective. *Depositional Rec.* 6, 605–624. doi:10.1002/dep2.109
- Fischer, M. D., and Uenzelmann-Neben, G. (2018a). Late Cretaceous Onset of Current Controlled Sedimentation in the African-Southern Ocean Gateway. *Mar. Geology*. 395, 380–396. doi:10.1016/j.margeo.2017.11.017
- Fischer, M. D., and Uenzelmann-Neben, G. (2018b). Neogene Modifications of Circulation in the Northeastern African-Southern Ocean Gateway. *Geochem. Geophys. Geosyst.* 19, 4673–4693. doi:10.1029/2018GC007644
- Flood, R. D. (1988). A lee Wave Model for Deep-Sea Mudwave Activity. *Deep Sea Res. A. Oceanographic Res. Pap.* 35, 973–983. doi:10.1016/0198-0149(88)90071-4
- Flood, R. D., and Shor, A. N. (1988). Mud Waves in the Argentine Basin and Their Relationship to Regional Bottom Circulation Patterns. *Deep Sea Res. Part A. Oceanographic Res. Pap.* 35, 943–971. doi:10.1016/0198-0149(88)90070-2
- Fonnesu, M., Haughton, P., Felletti, F., and McCaffrey, W. (2015). Short Length-Scale Variability of Hybrid Event Beds and its Applied Significance. *Mar. Pet. Geology*. 67, 583–603. doi:10.1016/j.marpetgeo.2015.03.028
- Fonnesu, M., Palermo, D., Galbiati, M., Marchesini, M., Bonamini, E., and Bendias, D. (2020). A New World-Class Deep-Water Play-type, Deposited by the Syndepositional Interaction of Turbidity Flows and Bottom Currents: The Giant Eocene Coral Field in Northern Mozambique. *Mar. Pet. Geology*. 111, 179–201. doi:10.1016/J.MARPETGEO.2019.07.047
- Fossum, K., Morton, A. C., Dypvik, H., and Hudson, W. E. (2019). Integrated Heavy mineral Study of Jurassic to Paleogene Sandstones in the Mandawa Basin, Tanzania: Sediment Provenance and Source-To-Sink Relations. *J. Afr. Earth Sci.* 150, 546–565. doi:10.1016/j.jafrearsci.2018.09.009
- Franke, D., Jokat, W., Ladage, S., Stollhofen, H., Klimke, J., Lutz, R., et al. (2015). The Offshore East African Rift System: Structural Framework at the Toe of a Juvenile Rift. *Tectonics* 34, 2086–2104. doi:10.1002/2015TC003922
- Friedrich, O., Norris, R. D., and Erbacher, J. (2012). Evolution of Middle to Late Cretaceous Oceans-A 55 m.Y. Record of Earth's Temperature and Carbon Cycle. *Geology* 40, 107–110. doi:10.1130/G32701.1
- Fuhrmann, A., Kane, I. A., Clare, M. A., Ferguson, R. A., Schomacker, E., Bonamini, E., et al. (2020). Hybrid Turbidite-Drift Channel Complexes : An Integrated Multiscale Model. *Geology*. 46, 1–7. doi:10.1130/G47179.1/4967910/g47179.pdf
- Galy, V., France-Lanord, C., Beyssac, O., Faure, P., Kudrass, H., and Palhol, F. (2007). Efficient Organic Carbon Burial in the Bengal Fan Sustained by the Himalayan Erosional System. *Nature* 450, 407–410. doi:10.1038/nature06273
- García, M., Hernández-Molina, F. J., Llave, E., Stow, D. A. V., León, R., Fernández-Puga, M. C., et al. (2009). Contourite Erosive Features Caused by the Mediterranean Outflow Water in the Gulf of Cadiz: Quaternary Tectonic and Oceanographic Implications. *Mar. Geology*. 257, 24–40. doi:10.1016/j.margeo.2008.10.009
- Gardner, W. D., Tucholke, B. E., Richardson, M. J., and Biscaye, P. E. (2017). Benthic Storms, Nepheloid Layers, and Linkage with Upper Ocean Dynamics in the Western North Atlantic. *Mar. Geology*. 385, 304–327. doi:10.1016/j.margeo.2016.12.012
- Gervais, A., Savoye, B., Mulder, T., and Gonthier, E. (2006). Sandy Modern Turbidite Lobes: A New Insight from High Resolution Seismic Data. *Mar. Pet. Geology*. 23, 485–502. doi:10.1016/j.marpetgeo.2005.10.006
- Gonthier, E. G., Faugères, J.-C., and Stow, D. A. V. (1984). Contourite Facies of the Faro Drift, Gulf of Cadiz. *Geol. Soc. Lond. Spec. Publications* 15, 275–292. doi:10.1144/GSL.SP.1984.015.01.18
- Grundvåg, S.-A., Johannessen, E. P., Helland-Hansen, W., and Plink-Björklund, P. (2014). Depositional Architecture and Evolution of Progradationally Stacked Lobe Complexes in the Eocene Central Basin of Spitsbergen. *Sedimentology* 61, 535–569. doi:10.1111/sed.12067
- Gwiazda, R., Paull, C. K., Ussler, W., and Alexander, C. R. (2015). Evidence of Modern fine-grained Sediment Accumulation in the Monterey Fan from Measurements of the Pesticide DDT and its Metabolites. *Mar. Geology*. 363, 125–133. doi:10.1016/j.margeo.2015.02.006
- Habgood, E. L., Kenyon, N. H., Masson, D. G., Akhmetzhanov, A., Weaver, P. P. E., Gardner, J., et al. (2003). Deep-water Sediment Wave fields, Bottom Current Sand Channels and Gravity Flow Channel-Lobe Systems: Gulf of Cadiz, NE Atlantic. *Sedimentology* 50, 483–510. doi:10.1046/j.1365-3091.2003.00561.x
- Hansen, L. A. S., Hodgson, D. M., Pontén, A., Bell, D., and Flint, S. (2019). Quantification of Basin-Floor Fan Pinchouts: Examples from the Karoo Basin, South Africa. *Front. Earth Sci.* 7, 1–20. doi:10.3389/feart.2019.00012
- Haughton, P., Davis, C., McCaffrey, W., and Barker, S. (2009). Hybrid Sediment Gravity Flow Deposits - Classification, Origin and Significance. *Mar. Pet. Geology*. 26, 1900–1918. doi:10.1016/j.marpetgeo.2009.02.012
- Haughton, P. D. W., Barker, S. P., and McCaffrey, W. D. (2003). 'Linked' Debrisites in Sand-Rich Turbidite Systems - Origin and Significance. *Sedimentology* 50, 459–482. doi:10.1046/j.1365-3091.2003.00560.x
- Hernández-Molina, F. J., Campbell, S., Badalini, G., Thompson, P., Walker, R., Soto, M., et al. (2017). Large Bedforms on Contourite Terraces: Sedimentary and Conceptual Implications. *Geology* 46, 27–30. doi:10.1130/G39655.1
- Hernández-Molina, F. J., Llave, E., and Stow, D. A. V. (2008). Chapter 19 Continental Slope Contourites. *Dev. Sedimentology*, 379–408. doi:10.1016/S0070-4571(08)10019-X
- Hernández-Molina, F. J., Soto, M., Piola, A. R., Tomasini, J., Preu, B., Thompson, P., et al. (2016a). A Contourite Depositional System along the Uruguayan continental Margin: Sedimentary, Oceanographic and Paleooceanographic Implications. *Mar. Geology*. 378, 333–349. doi:10.1016/j.margeo.2015.10.008
- Hernández-Molina, F. J., Wählin, A., Bruno, M., Ercilla, G., Llave, E., Serra, N., et al. (2016b). Oceanographic Processes and Morphosedimentary Products along the Iberian Margins: A New Multidisciplinary Approach. *Mar. Geology*. 378, 127–156. doi:10.1016/j.margeo.2015.12.008
- Hessler, A. M., and Fildani, A. (2019). Deep-sea Fans: Tapping into Earth's Changing Landscapes. *J. Sediment. Res.* 89, 1171–1179. doi:10.2110/jsr.2019.64
- Hiscott, R. N. (1994). Loss of Capacity, Not Competence, as the Fundamental Process Governing Deposition from Turbidity Currents. *J. Sediment. Res.* 64, 209–214. doi:10.2110/jsr.64.209
- Hollister, C. D., and McCave, I. N. (1984). Sedimentation under Deep-Sea Storms. *Nature* 309, 220–225. doi:10.1038/309220a0
- Hopfauf, V., Spieß, V., and Geowissenschaften, F. (2001). A Three-Dimensional Theory for the Development and Migration of Deep Sea Sedimentary Waves.

- Deep Sea Res. Oceanographic Res. Pap.* 48, 2497–2519. doi:10.1016/S0967-0637(01)00026-7
- Howlett, D. M., Ge, Z., Nemeč, W., Gawthorpe, R. L., Rotevatn, A., and Jackson, C. A. L. (2019). Response of Unconfined Turbidity Current to Deep-water Fold and Thrust belt Topography: Orthogonal Incidence on Solitary and Segmented Folds. *Sedimentology* 66, 2425–2454. doi:10.1111/sed.12602
- Hudson, W. E., and Nicholas, C. J. (2014). The Pindi Group (Triassic to Early Jurassic Mandawa Basin, Southern Coastal Tanzania): Definition, Palaeoenvironment, and Stratigraphy. *J. Afr. Earth Sci.* 92, 55–67. doi:10.1016/j.jafrearsci.2014.01.005
- Jegou, I., Savoye, B., Pirmez, C., and Droz, L. (2008). Channel-mouth Lobe Complex of the Recent Amazon Fan: The Missing Piece. *Mar. Geology* 252, 62–77. doi:10.1016/j.margeo.2008.03.004
- Jobe, Z. R., Howes, N., Romans, B. W., and Covault, J. A. (2018). Volume and Recurrence of Submarine-Fan-Building Turbidity Currents. *Depositional Rec.* 4, 160–176. doi:10.1002/dep.242
- Jobe, Z. R., Lowe, D. R., and Morris, W. R. (2012). Climbing-ripple Successions in Turbidite Systems: Depositional Environments, Sedimentation Rates and Accumulation Times. *Sedimentology* 59, 867–898. doi:10.1111/j.1365-3091.2011.01283.x
- Kane, I. A., and Clare, M. A. (2019). Dispersion, Accumulation, and the Ultimate Fate of Microplastics in Deep-Marine Environments: A Review and Future Directions. *Front. Earth Sci.* 7, 1–27. doi:10.3389/feart.2019.00080
- Kane, I. A., and Pontén, A. S. M. (2012). Submarine Transitional Flow Deposits in the Paleogene Gulf of Mexico. *Geology* 40, 1119–1122. doi:10.1130/G33410.1
- Kane, I. A., Pontén, A. S. M., Vangdal, B., Eggenhuisen, J. T., Hodgson, D. M., and Sychala, Y. T. (2017). The Stratigraphic Record and Processes of Turbidity Current Transformation across Deep-marine Lobes. *Sedimentology* 64, 1236–1273. doi:10.1111/sed.12346
- Key, R. M., Smith, R. A., Smelror, M., Saether, O. M., Thorsnes, T., Powell, J. H., et al. (2008). Revised Lithostratigraphy of the Mesozoic-Cenozoic Succession of the Onshore Rovuma Basin, Northern Coastal Mozambique. *South. Afr. J. Geology* 111, 89–108. doi:10.2113/gssajg.111.1.89
- Khripounoff, A., Vangriesheim, A., Babonneau, N., Crassous, P., Dennielou, B., and Savoye, B. (2003). Direct Observation of Intense Turbidity Current Activity in the Zaire Submarine valley at 4000 M Water Depth. *Mar. Geology* 194, 151–158. doi:10.1016/S0025-3227(02)00677-1
- Khripounoff, A., Vangriesheim, A., Crassous, P., and Etoubleau, J. (2009). High Frequency of Sediment Gravity Flow Events in the Var Submarine canyon (Mediterranean Sea). *Mar. Geology* 263, 1–6. doi:10.1016/j.margeo.2009.03.014
- Kneller, B. C., and Branney, M. J. (1995). Sustained High-Density Turbidity Currents and the Deposition of Thick Massive Sands. *Sedimentology* 42, 607–616. doi:10.1111/j.1365-3091.1995.tb00395.x
- Kneller, B., Edwards, D., McCaffrey, W., and Moore, R. (1991). Oblique Reflection of Turbidity Currents. *Geol.* 19, 250. doi:10.1130/0091-7613(1991)019<0250:orotc>2.3.co;2
- Kneller, B., and McCaffrey, W. (1999). Depositional Effects of Flow Nonuniformity and Stratification within Turbidity Currents Approaching a Bounding Slope: Deflection, Reflection, and Facies Variation. *J. Sediment. Res.* 69, 980–991. doi:10.2110/jsr.69.980
- König, M., and Jokat, W. (2010). Advanced Insights into Magmatism and Volcanism of the Mozambique Ridge and Mozambique Basin in the View of New Potential Field Data. *Geophys. J. Int.* 180, 158–180. doi:10.1111/j.1365-246X.2009.04433.x
- König, M., and Jokat, W. (2006). The Mesozoic Breakup of the Weddell Sea. *J. Geophys. Res. Solid Earth* 111. doi:10.1029/2005jb004035
- Leinweber, V. T., and Jokat, W. (2012). The Jurassic History of the Africa-Antarctica Corridor - New Constraints from Magnetic Data on the Conjugate continental Margins. *Tectonophysics* 530-531, 87–101. doi:10.1016/j.tecto.2011.11.008
- Lewis, K. B. (1994). The 1500-Km-Long Hikurangi Channel: Trench-axis Channel that Escapes its Trench, Crosses a Plateau, and Feeds a Fan Drift. *Geo-Marine Lett.* 14, 19–28. doi:10.1007/BF01204467
- Locker, S. D., and Laine, E. P. (1992). Paleogene-Neogene Depositional History of the Middle U.S. Atlantic continental Rise: Mixed Turbidite and Contourite Depositional Systems. *Mar. Geology* 103, 137–164. doi:10.1016/0025-3227(92)90013-8
- Lowe, D. R. (1982). Sediment Gravity Flows: II Depositional Models with Special Reference to the Deposits of High-Density Turbidity Currents. *Sepm Jsr* 52, 279–297. doi:10.1306/212F7F31-2B24-11D7-8648000102C1865D
- Lowe, D. R., and Guy, M. (2000). Slurry-flow Deposits in the Britannia Formation (Lower Cretaceous), North Sea: A New Perspective on the Turbidity Current and Debris Flow Problem. *Sedimentology* 47, 31–70. doi:10.1046/j.1365-3091.2000.00276.x
- Lowe, D. R. (1975). Water Escape Structures in Coarse-Grained Sediments. *Sedimentology* 22, 157–204. doi:10.1111/j.1365-3091.1975.tb00290.x
- Lutjeharms, J. R. E. (2006). *The Agulhas Current*. Springer Berlin Heidelberg. doi:10.1007/3-540-37212-1
- Makoto Ito, M. (1996). Sandy Contourites of the Lower Kazusa Group in the Boso Peninsula, Japan: Kuroshio-Current-Influenced Deep-Sea Sedimentation in a Plio-Pleistocene Forearc Basin. *Sepm Jsr* 66. doi:10.1306/D42683B5-2B26-11D7-8648000102C1865D
- Marchès, E., Mulder, T., Cremer, M., Bonnel, C., Hanquiez, V., Gonthier, E., et al. (2007). Contourite Drift Construction Influenced by Capture of Mediterranean Outflow Water Deep-Sea Current by the Portimão Submarine canyon (Gulf of Cadiz, South Portugal). *Mar. Geology* 242, 247–260. doi:10.1016/j.margeo.2007.03.013
- Marchès, E., Mulder, T., Gonthier, E., Cremer, M., Hanquiez, V., Garlan, T., et al. (2010). Perched Lobe Formation in the Gulf of Cadiz: Interactions between Gravity Processes and Contour Currents (Algarve Margin, Southern Portugal). *Sediment. Geology* 229, 81–94. doi:10.1016/j.sedgeo.2009.03.008
- Marini, M., Milli, S., Ravnås, R., and Moscatelli, M. (2015). A Comparative Study of Confined vs. Semi-confined Turbidite Lobes from the Lower Messinian Laga Basin (Central Apennines, Italy): Implications for Assessment of Reservoir Architecture. *Mar. Pet. Geology* 63, 142–165. doi:10.1016/j.marpetgeo.2015.02.015
- Martin, E. E., MacLeod, K. G., Jiménez Berrocoso, A., and Bourbon, E. (2012). Water Mass Circulation on Demerara Rise during the Late Cretaceous Based on Nd Isotopes. *Earth Planet. Sci. Lett.* 327-328328, 111–120. doi:10.1016/j.epsl.2012.01.037
- Martin-Chivelet, J., Fregenal-Martínez, M. A., and Chacón, B. (2008). Chapter 10 Traction Structures in Contourites,” in *Dev. Sedimentology*, 159–182. doi:10.1016/S0070-4571(08)10010-3
- Maselli, V., Kneller, B., Taiwo, O. L., and Iacomini, D. (2019). Sea Floor Bedforms and Their Influence on Slope Accommodation. *Mar. Pet. Geology* 102, 625–637. doi:10.1016/j.marpetgeo.2019.01.021
- Masson, D. G., Wynn, R. B., and Bett, B. J. (2004). Sedimentary Environment of the Faroe-Shetland and Faroe Bank Channels, north-east Atlantic, and the Use of Bedforms as Indicators of Bottom Current Velocity in the Deep Ocean. *Sedimentology* 51, 1207–1241. doi:10.1111/j.1365-3091.2004.00668.x
- Mayall, M., Jones, E., and Casey, M. (2006). Turbidite Channel Reservoirs—Key Elements In Facies Prediction And Effective Development. *Marine Petrol. Geol.* 23 (8), 821–841. doi:10.1016/j.marpetgeo.2006.08.001
- McArdle, N. J., and Ackers, M. A. (2012). Understanding Seismic Thin-Bed Responses Using Frequency Decomposition and RGB Blending. *First Break* 30, 57–65. doi:10.3997/1365-2397.2012022
- McCaffrey, W., and Kneller, B. (2001). Process Controls on the Development of Stratigraphic Trap Potential on the Margins of Confined Turbidite Systems and Aids to Reservoir Evaluation. *Am. Assoc. Pet. Geol. Bull.* 85, 971–988. doi:10.1306/8626ca41-173b-11d7-8645000102c1865d
- McCave, I. N., Thornalley, D. J. R., and Hall, I. R. (2017). Relation of Sortable silt Grain-Size to Deep-Sea Current Speeds: Calibration of the 'Mud Current Meter'. *Deep Sea Res. Part Oceanographic Res. Pap.* 127, 1–12. doi:10.1016/j.dsr.2017.07.003
- McCave, I. N., and Tucholke, B. E. (1986). Deep Current-Controlled Sedimentation in the Western North Atlantic. in *In the Western North Atlantic Region*. Boulder, Colorado: Geological Society of North America, 451–468. doi:10.1130/DNAG-GNA-M.451
- McGinnis, J. P., and Hayes, D. E. (1995). *The Roles of Downslope and Along-Slope Depositional Processes: Southern Antarctic Peninsula Continental Rise*, 141–156. doi:10.1029/AR068p0141
- Miramontes, E., Eggenhuisen, J. T., Jacinto, R. S., Poneti, G., Pohl, F., Normandeau, A., et al. (2020a). Channel-levee Evolution in Combined Contour Current-Turbidity Current Flows from Flume Tank Experiments: REPLY. *Geology* 48, e508. doi:10.1130/G47885Y.1
- Miramontes, E., Eggenhuisen, J. T., Jacinto, R. S., Poneti, G., Pohl, F., Normandeau, A., et al. (2020b). Channel-levee Evolution in Combined

- Contour Current – Turbidity Current Flows from Flume-Tank Experiments. *Geology*, 48, 1–5. doi:10.1130/G47111.1
- Miramontes, E., Penven, P., Fierens, R., Droz, L., Toucanne, S., Jorry, S. J., et al. (2019). The Influence of Bottom Currents on the Zambezi Valley Morphology (Mozambique Channel, SW Indian Ocean): *In Situ* Current Observations and Hydrodynamic Modelling. *Mar. Geology*, 410, 42–55. doi:10.1016/j.margeo.2019.01.002
- Miramontes, E., Thiéblemont, A., Babonneau, N., Penven, P., Raisson, F., Droz, L., et al. (2021). Contourite and Mixed Turbidite-Contourite Systems in the Mozambique Channel (SW Indian Ocean): Link between Geometry, Sediment Characteristics and Modelled Bottom Currents. *Mar. Geology*, 437, 106502. doi:10.1016/j.MARGE0.2021.106502
- Moiroud, M., Pucéat, E., Donnadiou, Y., Bayon, G., Guiraud, M., Voigt, S., et al. (2016). Evolution of Neodymium Isotopic Signature of Seawater during the Late Cretaceous: Implications for Intermediate and Deep Circulation. *Gondwana Res.* 36, 503–522. doi:10.1016/j.gr.2015.08.005
- Mulder, T., and Alexander, J. (2001). The Physical Character of Subaqueous Sedimentary Density Flows and Their Deposits. *Sedimentology* 48, 269–299. doi:10.1046/j.1365-3091.2001.00360.x
- Mulder, T., Faugères, J.-C., and Gonthier, E. (2008). Chapter 21 Mixed Turbidite-Contourite Systems. *Dev. Sedimentology*, 435–456. doi:10.1016/S0070-4571(08)10021-8
- Murphy, D. P., and Thomas, D. J. (2012). Cretaceous Deep-Water Formation in the Indian Sector of the Southern Ocean. *Paleoceanography* 27, a–n. doi:10.1029/2011PA002198
- Murphy, D. P., and Thomas, D. J. (2013). The Evolution of Late Cretaceous Deep-Ocean Circulation in the Atlantic Basins: Neodymium Isotope Evidence from South Atlantic Drill Sites for Tectonic Controls. *Geochem. Geophys. Geosyst.* 14, 5323–5340. doi:10.1002/2013GC004889
- Mutti, E., Cunha, R. S., Bulhoes, É. M., Arienti, L. M., and Viana, A. R. (2014). “Contourites and Turbidites of the Brazilian Marginal Basins,” in *Search and Discovery Article*.
- Ortiz-Karpf, A., Hodgson, D. M., Jackson, C. A. L., and McCaffrey, W. D. (2017). Influence Of Seabed Morphology And Substrate Composition On Mass-Transport Flow Processes And Pathways: Insights From The Magdalena Fan, Offshore Colombia. *J. Sedimentary Res.* 87 (3), 189–209. doi:10.2110/jsr.2017.10
- Patacci, M., Haughton, P. D. W., and McCaffrey, W. D. (2015). Flow Behavior of Pondered Turbidity Currents. *J. Sediment. Res.* 85, 885–902. doi:10.2110/jsr.2015.59
- Patacci, M., Haughton, P. D. W., and McCaffrey, W. D. (2014). Rheological Complexity in Sediment Gravity Flows Forced to Decelerate against A Confining Slope, Braux, SE France. *J. Sediment. Res.* 84, 270–277. doi:10.2110/jsr.2014.26
- Piper, D. J. W., and Normark, W. R. (1983). Turbidite Depositional Patterns and Flow Characteristics, Navy Submarine Fan, California Borderland. *Sedimentology* 30, 681–694. doi:10.1111/j.1365-3091.1983.tb00702.x
- Pohl, F., Eggenhuisen, J. T., Kane, I. A., and Clare, M. A. (2020). Transport and Burial of Microplastics in Deep-Marine Sediments by Turbidity Currents. *Environ. Sci. Technol.* 54, 4180–4189. doi:10.1021/acs.est.9b07527
- Pohl, F., Eggenhuisen, J. T., Tilston, M., and Cartigny, M. J. B. (2019). New Flow Relaxation Mechanism Explains Scour fields at the End of Submarine Channels. *Nat. Commun.* 10, 4425. doi:10.1038/s41467-019-12389-x
- Porten, K. W., Warchol, M. J., and Kane, I. A. (2019). Formation of Detrital clay Grain coats by Dewatering of Deep-Water Sands and Significance for Reservoir Quality. *J. Sediment. Res.* 89, 1231–1249. doi:10.2110/jsr.2019.65
- Poulsen, C. J., Barron, E. J., Arthur, M. A., and Peterson, W. H. (2001). Response of the Mid-Cretaceous Global Oceanic Circulation to Tectonic and CO₂ forcings. *Paleoceanography* 16, 576–592. doi:10.1029/2000PA000579
- Poulsen, C. J., Gendaszek, A. S., and Jacob, R. L. (2003). Did the Rifting of the Atlantic Ocean Cause the Cretaceous thermal Maximum? *Geol* 31, 115. doi:10.1130/0091-7613(2003)031<0115:dtrota>2.0.co;2
- Prather, B. E., O’Byrne, C., Pirmez, C., and Sylvester, Z. (2016). Sediment Partitioning, continental Slopes and Base-Of-Slope Systems. *Basin Res.* 29, 394–416. doi:10.1111/bre.12190
- Prather, B. E., Pirmez, C., and Winker, C. D. (2012). “Stratigraphy of Linked Intraslope Basins: Brazos–Trinity System Western Gulf of Mexico,” in *Application of the Principles of Seismic Geomorphology to Continental-Slope and Base-Of-Slope Systems: Case Studies from Seafloor and Near-Seafloor Analogues*. Tulsa, Oklahoma: SEPM Society for Sedimentary Geology, 83–109. doi:10.2110/pec.12.99.0083
- Prélat, A., Hodgson, D. M., and Flint, S. S. (2009). Evolution, Architecture and Hierarchy of Distributary Deep-Water Deposits: a High-Resolution Outcrop Investigation from the Permian Karoo Basin, South Africa. *Sedimentology* 56, 2132–2154. doi:10.1111/j.1365-3091.2009.01073.x
- Prélat, A., Covault, J. A., Hodgson, D. M., Fildani, A., and Flint, S. S. (2010). Intrinsic Controls on the Range of Volumes, Morphologies, and Dimensions of Submarine Lobes. *Sediment. Geology*, 232, 66–76. doi:10.1016/j.sedgeo.2010.09.010
- Preu, B., Hernández-Molina, F. J., Violante, R., Piola, A. R., Paterlini, C. M., Schwenk, T., et al. (2013). Morphosedimentary and Hydrographic Features of the Northern Argentine Margin: The Interplay between Erosive, Depositional and Gravitational Processes and its Conceptual Implications. *Deep Sea Res. Part Oceanographic Res. Pap.* 75, 157–174. doi:10.1016/j.dsr.2012.12.013
- Preu, B., Schwenk, T., Hernández-Molina, F. J., Violante, R., Paterlini, M., Krastel, S., et al. (2012). Sedimentary Growth Pattern on the Northern Argentine Slope: The Impact of North Atlantic Deep Water on Southern Hemisphere Slope Architecture. *Mar. Geology*, 329–331, 113–125. doi:10.1016/j.margeo.2012.09.009
- Rabouille, C., Dennielou, B., Baudin, F., Raimonet, M., Droz, L., Khripounoff, A., et al. (2019). Carbon and Silica Megasink in Deep-Sea Sediments of the Congo Terminal Lobes. *Quat. Sci. Rev.* 222, 105854. doi:10.1016/j.quascirev.2019.07.036
- Reeves, C. V., Teasdale, J. P., and Mahanjane, E. S. (2016). Insight into the Eastern Margin of Africa from a New Tectonic Model of the Indian Ocean. *Geol. Soc. Lond. Spec. Publications* 431, 299–322. doi:10.1144/SP431.12
- Reeves, C. V. (2018). The Development of the East African Margin during Jurassic and Lower Cretaceous Times: a Perspective from Global Tectonics. *Pet. Geosci.* 24, 41–56. doi:10.1144/petgeo2017-021
- Robinson, S. A., Murphy, D. P., Vance, D., and Thomas, D. J. (2010). Formation of “Southern Component Water” in the Late Cretaceous: Evidence from Nd-Isotopes. *Geology* 38, 871–874. doi:10.1130/G31165.1
- Robinson, S. A., and Vance, D. (2012). Widespread and Synchronous Change in Deep-Ocean Circulation in the North and South Atlantic during the Late Cretaceous. *Paleoceanography* 27, a–n. doi:10.1029/2011PA002240
- Romans, B. W., Castelltort, S., Covault, J. A., Fildani, A., and Walsh, J. P. (2016). Environmental Signal Propagation in Sedimentary Systems across Timescales. *Earth-Science Rev.* 153, 7–29. doi:10.1016/j.earscirev.2015.07.012
- Salles, L., Ford, M., and Joseph, P. (2014). Characteristics of Axially-Sourced Turbidite Sedimentation on an Active Wedge-Top basin (Annot Sandstone, SE France). *Mar. Pet. Geology*, 56, 305–323. doi:10.1016/j.marpetgeo.2014.01.020
- Salman, G., and Abdula, I. (1995). Development of the Mozambique and Rovuma Sedimentary Basins, Offshore Mozambique. *Sediment. Geology*, 96, 7–41. doi:10.1016/0037-0738(95)00125-R
- Sansom, P. (2018). Hybrid Turbidite-Contourite Systems of the Tanzanian Margin. *Pet. Geosci.* 24, 258–276. doi:10.1144/petgeo2018-044
- Shanmugam, G., Spalding, T. D., and Rofheart, D. H. (1993). Process Sedimentology and Reservoir Quality of Deep-Marine Bottom-Current Reworked Sands (Sandy Contourites): An Example from the Gulf of Mexico. *Am. Assoc. Pet. Geol. Bull.* 77, 1241–1259. doi:10.1306/bdff8e52-1718-11d7-8645000102c1865d
- Sinclair, H. D., and Tomasso, M. (2002). Depositional Evolution of Confined Turbidite Basins. *J. Sediment. Res.* 72, 451–456. doi:10.1306/111501720451
- Smelror, M., Fossum, K., Dypvik, H., Hudson, W., and Mweneinda, A. (2018). Late Jurassic-Early Cretaceous Palynostratigraphy of the Onshore Mandawa Basin, southeastern Tanzania. *Rev. Palaeobotany Palynology* 258, 248–255. doi:10.1016/J.REVPALBO.2018.09.001
- Smelror, M., Key, R. M., Smith, R. A., and Njange, F. (2008). Late Jurassic and Cretaceous Palynostratigraphy of the Onshore Rovuma Basin, Northern Mozambique. *Palynology* 32, 63–76.
- Sømme, T. O., Helland-Hansen, W., Martinsen, O. J., and Thurmond, J. B. (2009). Relationships between Morphological and Sedimentological Parameters in Source-To-Sink Systems: a Basis for Predicting Semi-quantitative Characteristics in Subsurface Systems. *Basin Res.* 21, 361–387. doi:10.1111/j.1365-2117.2009.00397.x
- Somme, T. O., Piper, D. J. W., Deptuck, M. E., and Helland-Hansen, W. (2011). Linking Onshore-Offshore Sediment Dispersal in the Golo Source-To-Sink System (Corsica, France) during the Late Quaternary. *J. Sediment. Res.* 81, 118–137. doi:10.2110/jsr.2011.11

- Southern, S. J., Kane, I. A., Warchoř, M. J., Porten, K. W., and McCaffrey, W. D. (2017). Hybrid Event Beds Dominated by Transitional-Flow Facies: Character, Distribution and Significance in the Maastrichtian Springar Formation, north-west Voring Basin, Norwegian Sea. *Sedimentology* 64, 747–776. doi:10.1111/sed.12323
- Soutter, E. L., Bell, D., Cumberpatch, Z. A., Ferguson, R. A., Sychala, Y. T., Kane, I. A., et al. (2021). The Influence of Confining Topography Orientation on Experimental Turbidity Currents and Geological Implications. *Front. Earth Sci.* 8, 1–25. doi:10.3389/feart.2020.540633
- Soutter, E. L., Kane, I. A., Fuhrmann, A., Cumberpatch, Z. A., and Huuse, M. (2019). The Stratigraphic Evolution of Onlap in Siliciclastic Deep-Water Systems: Autogenic Modulation of Allogenic Signals. *J. Sediment. Res.* 89, 890–917. doi:10.2110/jsr.2019.49
- Sychala, Y. T., Hodgson, D. M., Pr elat, A., Kane, I. A., Flint, S. S., and Mountney, N. P. (2017). Frontal and Lateral Submarine Lobe Fringes: Comparing Sedimentary Facies, Architecture and Flow Processes. *J. Sediment. Res.* 87, 75–96. doi:10.2110/jsr.2017.2
- Stevenson, C. J., Jackson, C. A.-L., Hodgson, D. M., Hubbard, S. M., and Eggenhuisen, J. T. (2015). Deep-Water Sediment Bypass. *J. Sediment. Res.* 85, 1058–1081. doi:10.2110/jsr.2015.63
- Stevenson, C. J., Peakall, J., Hodgson, D. M., Bell, D., and Privat, A. (2020). TB or Not TB: Banding in Turbidite Sandstones. *J. Sediment. Res.* 90, 821–842. doi:10.2110/jsr.2020.43
- Stow, D. A. V., and Faug eres, J.-C. (2008). Chapter 13 Contourite Facies and the Facies Model. *Dev. Sedimentology*, 223–256. doi:10.1016/S0070-4571(08)10013-9
- Stow, D. A. V., Hern andez-Molina, F. J., Llave, E., Sayago-Gil, M., D iaz del R ıo, V., and Branson, A. (2009). Bedform-velocity Matrix: The Estimation of Bottom Current Velocity from Bedform Observations. *Geology* 37, 327–330. doi:10.1130/G25259A.1
- Stow, D. A. V., Hunter, S., Wilkinson, D., and Hern andez-Molina, F. J. (2008). Chapter 9 the Nature of Contourite Deposition. *Dev. Sedimentology*, 143–156. doi:10.1016/S0070-4571(08)10009-7
- Sumner, E. J., Talling, P. J., and Amy, L. A. (2009). Deposits of Flows Transitional between Turbidity Current and Debris Flow. *Geology* 37, 991–994. doi:10.1130/G30059A.1
- Symons, W. O., Sumner, E. J., Paull, C. K., Cartigny, M. J. B., Xu, J. P., Maier, K. L., et al. (2017). A New Model for Turbidity Current Behavior Based on Integration of Flow Monitoring and Precision Coring in a Submarine canyon. *Geology* 45, 367–370. doi:10.1130/G38764.1
- Talling, P. J. (2013). Hybrid Submarine Flows Comprising Turbidity Current and Cohesive Debris Flow: Deposits, Theoretical and Experimental Analyses, and Generalized Models. *Geosphere* 9, 460–488. doi:10.1130/GES00793.1
- Talling, P. J., Masson, D. G., Sumner, E. J., and Malgesini, G. (2012). Subaqueous Sediment Density Flows: Depositional Processes and deposit Types. *Sedimentology* 59, 1937–2003. doi:10.1111/j.1365-3091.2012.01353.x
- Thi blemont, A., Hern andez-Molina, F. J., Miramontes, E., Raison, F., and Penven, P. (2019). Contourite Depositional Systems along the Mozambique Channel: The Interplay between Bottom Currents and Sedimentary Processes. *Deep Sea Res. Part Oceanographic Res. Pap.* 147, 79–99. doi:10.1016/j.dsr.2019.03.012
- Thi blemont, A., Hern andez-Molina, F. J., Ponte, J.-P., Robin, C., Guillocheau, F., Cazzola, C., et al. (2020). Seismic Stratigraphic Framework and Depositional History for Cretaceous and Cenozoic Contourite Depositional Systems of the Mozambique Channel, SW Indian Ocean. *Mar. Geology*. 425, 106192. doi:10.1016/j.margeo.2020.106192
- Thran, A. C., Dutkiewicz, A., Spence, P., and M uller, R. D. (2018). Controls on the Global Distribution of Contourite Drifts: Insights from an Eddy-Resolving Ocean Model. *Earth Planet. Sci. Lett.* 489, 228–240. doi:10.1016/j.epsl.2018.02.044
- Tinterri, R., Muzzi Magalhaes, P., Tagliaferri, A., and Cunha, R. S. (2016). Convolute Laminations and Load Structures in Turbidites as Indicators of Flow Reflections and Decelerations against Bounding Slopes. Examples from the Marnoso-Arenacea Formation (Northern Italy) and Annot Sandstones (South Eastern France). *Sediment. Geology*. 344, 382–407. doi:10.1016/j.sedgeo.2016.01.023
- Uenzelmann-Neben, G., Weber, T., Gr utzner, J., and Thomas, M. (2017). Transition from the Cretaceous Ocean to Cenozoic Circulation in the Western South Atlantic - A Twofold Reconstruction. *Tectonophysics* 716, 225–240. doi:10.1016/j.tecto.2016.05.036
- Ullgren, J. E., van Aken, H. M., Ridderinkhof, H., and de Ruijter, W. P. M. (2012). The Hydrography of the Mozambique Channel from Six Years of Continuous Temperature, Salinity, and Velocity Observations. *Deep Sea Res. Part Oceanographic Res. Pap.* 69, 36–50. doi:10.1016/j.dsr.2012.07.003
- Voigt, S., Jung, C., Friedrich, O., Frank, M., Teschner, C., and Hoffmann, J. (2013). Tectonically Restricted Deep-Ocean Circulation at the End of the Cretaceous Greenhouse. *Earth Planet. Sci. Lett.* 369–370/370, 169–177. doi:10.1016/j.epsl.2013.03.019–
- Warratz, G., Schwenk, T., Voigt, I., Bozzano, G., Henrich, R., Violante, R., et al. (2019). Interaction of a deep-sea current with a blind submarine canyon (Mar del Plata Canyon, Argentina). *Mar. Geology*. 417, 106002. doi:10.1016/j.margeo.2019.106002
- Wynn, R. B., and Masson, D. G. (2008). Chapter 15 Sediment Waves and Bedforms. *Dev. Sedimentol.* 60, 289–300. doi:10.1016/S0070-4571(08)10015-2
- Wynn, R. B., and Stow, D. A. V. (2002a). Classification and Characterisation of Deep-Water Sediment Waves. *Mar. Geology*. 192, 7–22. doi:10.1016/S0025-3227(02)00547-9
- Wynn, R. B., and Stow, D. A. V. (2002b). Classification and Characterisation of Deep-Water Sediment Waves. *Mar. Geology*. 192, 7–22. doi:10.1016/s0025-3227(02)00547-9

Conflict of Interest: ES and AP are employed by Equinor ASA.

The remaining authors declare that the research was conducted in the absence of any commercial or financial relationships that could be construed as a potential conflict of interest.

Publisher’s Note: All claims expressed in this article are solely those of the authors and do not necessarily represent those of their affiliated organizations, or those of the publisher, the editors, and the reviewers. Any product that may be evaluated in this article, or claim that may be made by its manufacturer, is not guaranteed or endorsed by the publisher.

Copyright   2022 Fuhrmann, Kane, Schomacker, Clare and Pont en. This is an open-access article distributed under the terms of the Creative Commons Attribution License (CC BY). The use, distribution or reproduction in other forums is permitted, provided the original author(s) and the copyright owner(s) are credited and that the original publication in this journal is cited, in accordance with accepted academic practice. No use, distribution or reproduction is permitted which does not comply with these terms.